Carbohydrate Polymers 277 (2022) 118895

Contents lists available at ScienceDirect

Carbohydrate Polymers

journal homepage: www.elsevier.com/locate/carbpol

Polysaccharide-based hydrogels crosslink density equation: A rheological and LF-NMR study of polymer-polymer interactions

Tilen Kopač [a], Michela Abrami [b], Mario Grassi [b], Aleš Ručigaj [a], Matjaž Krajnc [a,*]

[a] University of Ljubljana, Faculty of Chemistry and Chemical Technology, Večna pot 113, SI-1000 Ljubljana, Slovenia
[b] University of Trieste, Department of Engineering and Architecture, Building B, via Valerio 6, I-34127 Trieste, Italy

ARTICLE INFO

Keywords:
Crosslink density
Rheology
LF-NMR
Hydrogel interactions
Mathematical modeling

ABSTRACT

A simple relation between pendant groups of polymers in hydrogels is introduced to determine the crosslink density of (complex) hydrogel systems (mixtures of 2,2,6,6-tetramethylpiperidine-1-oxyl (TEMPO) modified nanocellulose, alginate, scleroglucan and Laponite in addition of crosslinking agents). Furthermore, the rheological properties and their great potential connection to design complex hydrogel systems with desired properties have been thoroughly investigated. Hydrogel structures governing internal friction and flow resistance were described by the predominant effect of ionic, hydrogen, and electrostatic interactions. The relationship between rheological properties and polymer-polymer interactions in the hydrogel network is explained and expressed in a new mathematical model for determining the crosslink density of (crosslinked) hydrogels based on single or mixture of polymer systems. In the end, the combined used of rheology and low field nuclear magnetic resonance spectroscopy (LF-NMR) for the characterization of hydrogel networks is developed.

1. Introduction

Hydrogels belong to a group of intelligent materials (Mahinroosta et al., 2018) that, due to their many unique mechanical, physical and chemical properties, have found a significant role in a wide applicability in many fields (Chen et al., 2019; Zinge & Kandasubramanian, 2020). In recent years, there has been an increasing interest in researching the use of hydrogels in medicine (Rosiak & Yoshii, 1999), pharmacy (Peppas et al., 2000), including clinical studies, diagnostics and cell immobilization (Hoare & Kohane, 2008), separation of biomolecules or cells (Wang et al., 1993), microfluidics (Goy et al., 2019), tissue engineering (Drury & Mooney, 2003), food industry (Andrade Batista et al., 2018), etc. The study of the characterization of the hydrogel structure is therefore very important and advantageous in all the mentioned areas. Knowledge of the properties of polymers and the resulting hydrogels, as well as the response of hydrogel properties to the method of preparation, polymer concentration and concentration of crosslinking agent, can significantly contribute to the development of new hydrogel systems and increase the practical value (Kopač et al., 2020).

The hydrogel structure is formed when enough polymer chains are interconnected (in crosslink points) to create a hydrogel network that begins to swell due to hydrophilic nature (Ahmed, 2015). Therefore, the crosslink density is a major factor in the design of hydrogels with the desired properties. Modeling of controlled drug release from hydrogels (drug delivery systems) has been the subject of considerable research over the last 50 years (Manga & Jha, 2017). However, significantly fewer models have been developed to predict mechanical hydrogel properties such as crosslink density and shear modulus. To date, the only known mathematical models for predicting crosslink density with respect to the properties of constituent polymers are Peppas-Merrill equation Eq. (A.1) in Appendix A (Carr & Peppas, 2009), which is a modification of the Flory-Rehner equation Eq. (A.2) in Appendix A (Bruck, 1961). The models describe the mixing of polymer and liquid molecules according to the theory of equilibrium swelling due to the crosslink density. They are based on the Flory-Rehner theory, which specifies a change in free energy when a polymer gel swells (Bruck, 1961; Carr & Peppas, 2009). Eq. (A.1) and (A.2) in Appendix A only apply to simple solvent-swellable polymer systems. On the other hand, for more sophisticated polymer systems, it is often difficult to determine all the necessary parameters in Eq. (A.1) and (A.2) in Appendix A, especially the Flory parameter, reflecting the need for more recent adaptations.

Single polymer hydrogels have been well studied and are already being developed for practical use (Das & Pal, 2015). However, the

* Corresponding author.
E-mail address: matjaz.krajnc@fkkt.uni-lj.si (M. Krajnc).

https://doi.org/10.1016/j.carbpol.2021.118895
Received 1 September 2021; Received in revised form 29 October 2021; Accepted 11 November 2021
Available online 15 November 2021

development of delivery systems for many applications nowadays requires careful planning of the desired properties of the product. In order to increase the various properties to achieve the desired properties of the target application, the current trend focuses on the preparation of hydrogel mixtures of at least two polymers. By mixing the basic polymers, hydrogen, van der Waals and electrostatic interactions are formed between the polymer chains, which increase the crosslink density and impart the viscoelastic and thixotropic properties to the resulting complex (Liang et al., 2019) that are unique characteristic of hydrogel systems (Liang et al., 2020). This creates a rheological synergism between the basic polymers that enhances the properties of the constituent polymers that do not form the three-dimensional (3D) hydrogel structure. To even further extend the hydrogel properties, different crosslinking agents have been added to complex systems consisting of mixtures of different polymers. The mathematical description of crosslink density in such chemically or ionically crosslinked complex polymer networks is therefore difficult to be described by Eq. (A.1) and (A.2) in Appendix A. Another non-ideal feature of hydrogels, which is not considered in the equation Peppas-Merrill, is spatial gel inhomogeneity, as hydrogels always exhibit an inhomogeneous crosslink density distribution (Abrami et al., 2018; Fanesi et al., 2018). While crosslink density of hydrogels can be described by rheological measurements, the gel inhomogeneity can be effectively determined by LF-NMR analysis (Fanesi et al., 2018).

Accordingly, in this work, the combined use of rheology and LF-NMR is exploited to describe the structural properties of hydrogels giving the necessary fundamentals for mathematical model development. The mechanical properties of different hydrogel systems based on TEMPO nanocellulose (TOCNF), sodium alginate (ALG), scleroglucan (SCLG) and Laponite (LAP) were tested. The rheological oscillatory tests were performed to study polymer-polymer interactions (ionic, hydrogen, and other electrostatic interactions, etc.) which are the main factor for hydrogel to crosslink and to form a hydrogel network (3D structure). Following that, it is recommended to know the structural formula (Scheme 1) of TOCNF (Isogai et al., 2011; Liang et al., 2020), ALG (Homayouni et al., 2007), SCLG (Coviello et al., 2005) and LAP (Ruzicka & Zaccarelli, 2011) with special emphasis on substituent groups in order to understand the possible formation of chemical bonds in a process of gel formation. Based on these results, we hypothesize that the mathematical model can successfully predict crosslink density by knowing possible polymer-polymer interactions associated with the selected polymer and crosslinker used.

ALG and TOCNF are anionic biopolymers which, in presence of divalent cations, form strong ionic interactions due to carboxyl pendant groups on the surface of polymer. Ionic bonds are significantly stronger than hydrogen and other electrostatic forces in hydrogel network so that ionic bonds play a pivotal role in determination of crosslink density in most cases. On the other hand, SCLG and TOCNF single polymer hydrogel systems (in absence of crosslinking agent) predominantly form hydrogen interactions between polymer chains. Therefore, it is assumed that hydrogen and electrostatic interactions predominantly determine the viscoelastic properties of hydrogel structures even at low concentrations of ionic bonds. In the end, LAP mostly forms electrostatic interactions (Park et al., 2020) which is the main reason why it has important effect on crosslink density in mixtures with anionic polymers. In the end, the combined use of rheology and LF-NMR enables understanding the polymer-polymer interactions in hydrogel network, which were exploited to develop a new equation for calculation the crosslink density of complex hydrogel systems.

2. Experimental

2.1. Materials

The TEMPO oxidized nanofibrillated cellulose, a linear polysaccharide composed of anhydroglucose repeating units linked by β-(1–4) glycosidic bonds (French, 2017), was purchased from The Process Development Centre, University of Maine (UMaine PDC), USA. According to specifications given by the producer, the material $[(C_6H_{10}O_5)_x(C_6H_9O_4COONa)_y]$ is characterized by a carboxylation level of 0.2–2 mmol/g solids, which was experimentally determined in the literature (Kopač et al., 2021) at 1.2 mmol/g, and a pK_a of substituent group at 3.9. The fiber dimensions are classified between 20 and 50 nm in width and lengths of up to several microns. The material was purchased in freeze-dried powder with a density of 1.5 g/cm^3, which forms a gel structure in water (1–3 wt%) with a density of 1.0 g/cm^3.

Sodium alginate, a polysaccharide made up of high α-L-*guluronic* acid (G) content ~70% and (1–4)-linked β-d-mannuronic acid (M) monomers with molecular weight of 20–60 kDa, were supplied by Sigma-Aldrich (St. Louis, USA).

Scleroglucan Actigum CS 11 was purchased from Cargill France SAS, France. The structure consists of the main chain of (1,3)-linked β-D-glucopyranosyl units, bearing a single β-D-glucopyranosyl unit-linked (1,6). The supplier provides 99%min purity, and the average molecular weight M_w is $1.2{\cdot}10^6$.

Laponite XLG was provided by BYK-Chemie GmbH, Germany. According to the supplier specifications, it is a synthetic layered silicate with a low heavy metals content, it is insoluble in water but hydrates and swells giving clear and colorless colloidal dispersions in water. At concentrations of 2 wt% or greater in water, highly thixotropic gels are obtained. It obtains a high surface area (BET) of 800 m^2/g. Laponite nanoparticles are defined as disk-shaped crystals with an average

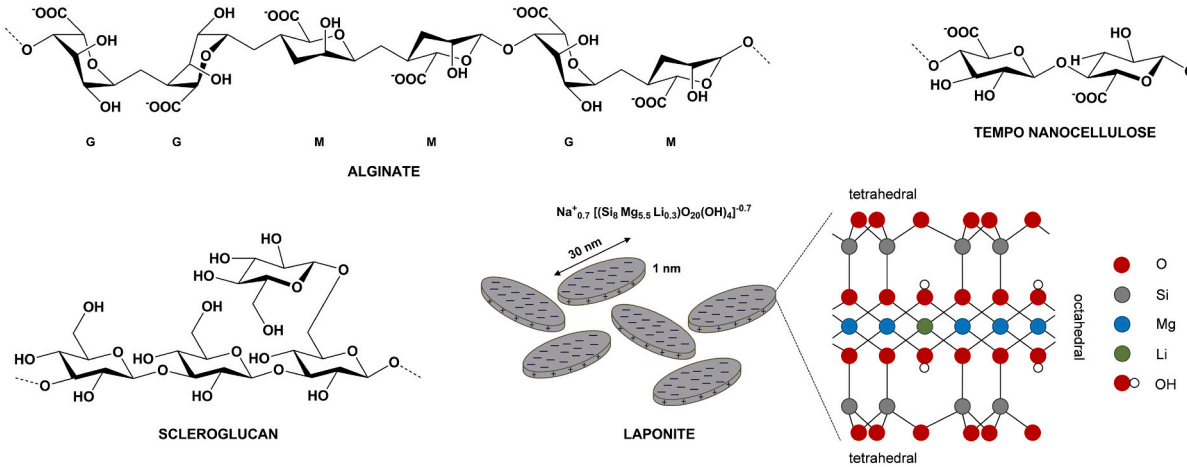

Scheme 1. Chemical structures of the alginate, TEMPO nanocellulose, scleroglucan and Laponite.

diameter of 30 nm and a thickness of 1 nm.

Calcium chloride was as received from Merck (Darmstadt, Germany) and sodium azide (NaN_3, an assay of ≥99.5%) was supplied by Sigma-Aldrich (St. Louis, USA).

2.2. Hydrogel samples preparation

Single hydrogel systems (only one type of biopolymer content) were prepared by dispersing constituent biopolymer in demineralized water at concentrations of 1–3 wt%. The water contained 0.02 wt% sodium azide to prevent eventual microbiological contamination. The dispersion was stirred for 2 h on a propeller stirrer at max 500 rpm. The dispersion was then exposed to an ultrasonic bath for 1 h to achieve better dispersion of solid particles. After sonication, stirring was provided at 750 rpm for 12 h. The prepared constituent biopolymer dispersions were kept in the fridge at a temperature of 4.2 °C for 15 days to establish typical 3D hydrogel structure and to avoid the effect of aging (according to the studies in (Lapasin et al., 2017; Šebenik et al., 2019)).

Single hydrogel systems were blended in different weight ratios (from 0.9 to 0.1) on a four-blade propeller stirrer for a further 2 h mixing. Single hydrogel blends were subsequently crosslinked by linking the carboxyl groups of anionic polymers via calcium ions. In this case, the prepared samples are denoted as complex (interpenetrated) hydrogel systems. Blends of single hydrogels were simply poured into a 3D printed mold of the same dimensions as the measuring plate on the rheometer (diameter of 5 cm and thickness of 1 mm). In the case of complex hydrogel systems, samples were further on sprayed (to achieve uniform crosslinker distribution over the specimen) with an aqueous solution of calcium chloride in various concentrations (data are available in Table S2). The volume of added crosslinking agent solution was equal to the volume of the hydrogel blends. The prepared complex neutral and anionic biopolymer-based hydrogel systems were maintained in a refrigerator at 4.2 °C for 24 h to establish the final hydrogel structure (time required for participation of all Ca^{2+} ions in crosslinking process). The list of produced systems can be seen in Table S2.

2.3. Characterization

2.3.1. Rheological measurements

Rheological measurements were performed on an Anton Paar Physica MCR 301 rheometer at a temperature of 25 °C. The measuring equipment used was a crosshatched plate with a diameter of 50 mm (PP50/P2). Samples were prepared to correspond to a thickness of 1 ± 0.1 mm between the plates. Rheological measurements include oscillatory (amplitude and frequency) tests. Amplitude tests were performed at constant oscillation frequency 1 Hz in order to determine the linear viscoelastic range within which frequency tests were performed (at a constant strain of 0.1% (Lundahl et al., 2018)). The oscillation frequencies varied from 100 to 0.01 Hz. The results of frequency tests called mechanical spectra were fitted with generalized Maxwell model:

$$G' = G_e + \sum_{i=1}^{n} \frac{G_i \lambda_i^2 \omega^2}{1 + \lambda_i^2 \omega^2} \tag{1}$$

$$G'' = \sum_{i=1}^{n} \frac{G_i \lambda_i \omega}{1 + \lambda_i^2 \omega^2} \tag{2}$$

where G_e is the equilibrium modulus, G_i are Maxwell elements spring constant which determine relaxation modules, λ_i is the corresponding relaxation time of the i^{th} Maxwell element, n is the number of considered Maxwell elements and ω is frequency. Furthermore, the shear modulus G can be estimated from the sum of the Maxwell elastic elements:

$$G = \sum_{k=1}^{n} G_k + G_e \tag{3}$$

where G_e and G_k are Maxwell's elements spring constants.

2.3.2. LF-NMR measurements

Typically, LF-NMR characterization of polymeric networks can be performed by looking at the magnetic relaxation of hydrogen belonging to polymeric chains, as nicely documented by Saalwachter (Saalwachter, 2003; Saalwachter, 2007; Saalwachter et al., 2013; Valentın et al., 2009). Alternatively, it is possible recording the relaxation of the hydrogen belonging to the solvent swelling the polymeric network as performed by other authors (Abrami et al., 2014; Abrami et al., 2019; Brownstein & Tarr, 1979; Chui et al., 1995; Jaeger et al., 2010; Li et al., 2015; Li et al., 2016; Scherer, 1994). While in the first case the use of deuterated solvents is mandatory to suppress the relaxation of solvent hydrogen (which, typically, in hydrogels represent the majority of system hydrogen (up to 99.5%)), in the second case, non-deuterated solvents have to be used. Indeed, this second approach aims to evaluate the effect of polymeric chains on the magnetic relaxation of solvent hydrogen (Chui et al., 1995; Scherer, 1994). In this paper, we decided to follow the second strategy to avoid the use of expensive deuterated solvents. All characterizations were performed at 25 °C by means of a Bruker Minispec mq20 (0.47 T, 20 MHz, Germany). The determination of the average water protons transverse (spin-spin) relaxation time inside the samples (T_{2m}) was performed according to the CPMG (Carr–Purcell–Meiboom–Gill) (Meiboom & Gill, 1958) sequence {90° [-τ-180°-τ (echo)]$_n$-T_R} with a 8.36 μs wide 90°pulse, τ = 0.25 ms, and T_R (sequences repetition rate) equal to 10 s.

LF-NMR characterization implies the introduction of a 1–2 mL of blend in NMR tube, then analysis proceeds and the output consist in the magnetization decay ($I(t)$) due to the magnetic relaxation of hydrogens belonging to water molecules contained in the sample. Then, $I(t)$ is fitted by means of a sum of decaying exponentials, each one characterized by a different time decay constant (T_{2i}) and weight (A_i) (Abrami et al., 2018; Fanesi et al., 2018):

$$\boldsymbol{I(t)} = \sum_{i=1}^{m} \boldsymbol{A_i e^{(-t/T_{2i})}} \tag{4}$$

The set of all the decay constants forms the decay spectrum or transverse-relaxation-time distribution (A_i,T_{2i}). Details of Eq. (4) fitting to experimental data are given in Supporting Materials. On the basis of Eq. (4), we can define the average value of the relaxation time (T_{2m}) and the average value of its inverse $(1/T_2)_m$ by (Abrami et al., 2018; Fanesi et al., 2018):

$$\begin{aligned} T_{2m} &= \sum_{i=1}^{m} A_i T_{2i} \Big/ \sum_{i=1}^{m} A_i ; A_{i\%} = 100 A_i \Big/ \sum_{i=1}^{m} A_i \left(\frac{1}{T_2}\right) m \\ &= \sum_{i=1}^{m} (A_i / T_{2i}) \Big/ \sum_{i=1}^{m} A_i \end{aligned} \tag{5}$$

while T_{2m} differs from $1/(1/T_2)_m$, we found the existence of a strong ($r = 0.982$, $p < 10^{-4}$) linear correlation (T_{2m} (ms) = (0.985 ± 0.01)*1/(1/T_2)$_m$) + (26.7 ± 4.7)) between T_{2m} and $1/(1/T_2)_m$ referring to our 90 systems.

LF-NMR measures the spin-spin relaxation time (T_{2m}) of the water hydrogen present in a liquid solution. T_{2m} is a very useful parameter to characterize soft materials. Indeed, T_{2m} value is inversely proportional to solid concentration (polymer, nanoparticles, nanofibers) and it also depends on the spatial organization of the solid fraction. Indeed, as water molecules near to solid surface relax faster than far ones (surface behaves as a magnetization absorber due to presence of impurities), T_{2m} is affected by the characteristics of the three-dimensional network such as the mesh size (Abrami et al., 2018; Fanesi et al., 2018).

As reported in the introduction, hydrogels always exhibit an inhomogeneous crosslink density distribution which is reflected in a mesh size distribution inside the network. In addition, the mesh size distribution (and consequently the crosslink density distribution) can be determined by substituting the average relaxation time T_{2m} with the

individual relaxation time T_{2i} (from the relaxation spectrum of the hydrogel sample giving T_{2m}) in Eq. (6). As for all our samples fast diffusion conditions (Brownstein & Tarr, 1979) are met and the combined effect on $(1/T_2)_m$ of the internal magnetic field gradient ΔG ($< 10^2$ T/m) and the water self-diffusion coefficient D (2.5×10^{-9} m^2/s) is negligible ($\approx 0.003\%$ of $1/T_{2,H2O}$), the determination of the (average) hydrogel network mesh size, ε, via LF-NMR is provided by Eq. (6) (Abrami et al., 2018; Coates et al., 1999) (see further comments on Eq. (6) in Appendix B).

$$\left(\frac{1}{T_2}\right)_m = \frac{1}{T_{2,H_2O}} + \frac{2\mathscr{M}}{\varepsilon\sqrt{\frac{1-0.58\varphi_p}{3\pi\varphi_p}}} \tag{6}$$

where $T_{2,H2O}$ is the relaxation time of free water protons (3000 ms at 25 °C and 20 MHz), φ_p is polymer volume fraction and $\mathscr{M}$ is relaxivity, dimensionally a velocity (length/time), that reflects the effect of polymeric chains on the water protons relaxation. Empirical parameter $\mathscr{M}$ can be determined by using the ε from the rheological measurements (Eq. (7)) or new developed mathematical model (Eq. (12)) considering correlation between crosslink density ρ_x and ε (Eq. (8)):

$$\rho_x = \frac{G}{RT}\left(\frac{\varphi_p}{\varphi_{p0}}\right)^{2/3} \tag{7}$$

$$\varepsilon = \sqrt[3]{\frac{6}{\pi\rho_x N_A}} \tag{8}$$

where G is shear modulus from Eq. (3), R is the universal gas constant, T is the temperature in K, φ_{p0} and φ_p are polymer volume fraction in the crosslinked conditions (reference conditions) and rheological measurement conditions (the gel could undergo swelling or shrink before the analysis) while N_A is the Avogadro number. The last term (φ_p/φ_{p0}) in Eq. (7) should in most cases be equal to 1. However, it sometimes happens (especially in the case of hydrogels with a high crosslink density - e.g., Ca^{2+} ions concentration over 1%) that due to sample compression before measurement on the rheometer the hydrogel loses some water, which changes the crosslink density in the crosslinked conditions.

3. Results and discussion

3.1. Models to describe crosslink density of hydrogels

To simplify somewhat the characterization of the hydrogel network, we have developed a mathematical model to predict the crosslink density (ρ_x) in complex hydrogel systems (mixtures of different polymers with the addition of crosslinking agents). The model is based on the amount of substituent groups of the polymers that can form hydrogen, ionic, electrostatic, and other covalent interactions between polymer chains, and thus create crosslinking points:

$$\rho_{x,max} = \frac{number\ of\ moles\ of\ crosslinks}{volume\ of\ hydrogel} = \frac{\overline{N}\, m_p}{2} \tag{9}$$

where $\overline{N}$ is substituent groups content (OH, COOH, NH_2, etc.) defined per gram of dry polymer [mmol/g] (two substituent groups can form one crosslink point) and m_p is the mass concentration of dry polymer in the solvent [g/m^3]. Eq. (9) represents the (theoretical) maximum value of crosslink density that can be achieved in particular hydrogel system.

3.1.1. Single polymer systems giving origin to hydrogels relaying on interchains hydrogen bonds

Considering a single-polymer hydrogel system crosslinked by hydrogen interactions between polymer chains (via OH groups), Eq. (9) is modified accordingly:

$$\rho_{x,hyd} = \frac{\overline{N_{hyd}}\,(m_p - m_{p0})}{2} a_{hyd} \tag{10}$$

where $\overline{N_{hyd}}$ is the amount of hydroxyl content on the surface per gram of dry polymer [mmol/g] and can be calculated mathematically using the same procedure as presented by Ho et al. (Ho et al., 2011). Furthermore, m_p and m_{p0} are the mass concentration of dry polymer in the solvent and a minimum mass concentration of polymer with the ability of hydrogel formation [g/m^3]. The lowest concentration of polymer that still forms the hydrogel m_{p0} can be determined experimentally (as in the article (Kopač et al., 2020)) or as adopted from the literature. The last parameter in Eq. (10) is the hydrogen bonds functionality affinity a_{hyd} [/] which defines the contribution of hydrogen bonds to the formation of a hydrogel network (the ability to form crosslinking points). As reported earlier, different interactions can form crosslinking points. Hydrogen interactions are the most common but are much weaker than ionic or covalent bonds. Therefore, the effect of hydrogen interactions is often negligible in the case of ionic and covalent crosslinking. What is more, the hydrogen bonds are only 197 pm long, making it impossible for all the hydroxyl groups on the polymer chains to find interaction together. The effect of hydrogen bond strength and functionality affinity is described by the parameter a_{hyd}, which was proved to be constant for all hydrogel systems with hydrogen interactions when the mechanical properties of gels are stable (final gels properties after the process of aging).

3.1.2. Ionically crosslinked hydrogel systems based on a single polymer containing carboxyl groups that form ionic interactions between polymers chains

The crosslink density of ionically crosslinked hydrogels depends predominant on the number of carboxyl groups on the surface of the polymer chains and the concentration of ionic crosslinking agent. The modification of Eq. (9) for ionically crosslinked hydrogels is shown in our previous study (Kopač et al., 2021):

$$\rho_{x,ion} = \frac{\overline{N_{ion}}\, m_p}{2} e^{-\frac{a_{ion}}{x}} \tag{11}$$

where $\overline{N_{ion}}$ is the amount of carboxyl content on the surface per gram of dry polymer [mmol/g] that participate in the crosslinking process (e.g. in ALG, only α-L-*guluronic* acid (70% content) is able to efficiently bind the Ca^{2+} crosslinker) and can usually be taken from the manufacturer's specification or determined experimentally by conductometric titration (Kopač et al., 2021), and x is the crosslinker concentration [wt%]. The a_{ion} is the functionality affinity [wt%] of the ionic crosslinking agent which refers to the tendency of a crosslinking agent ion (Ca^{2+} in our case) to create a connection (i.e., crosslink point) between two polymer chains (via carboxyl groups in our case). The characteristic ion-binding properties with the affinity for divalent ions increasing in the order of $Mg^{2+} \ll Ca^{2+} \ll Sr^{2+} \ll Ba^{2+}$ which means the a_{ion} hypothetically decreases in the same way. The development of Eq. (11) with the detailed discussion on the determination of a_{ion} is presented in our previous studies (Kopač et al., 2020; Kopač et al., 2021). The a_{ion} value of calcium ions as crosslinking agents was determined to be 0.55 wt%.

3.1.3. Complex (ionically crosslinked) hydrogel systems based on a mixture of different polymers (simultaneous effect of hydrogen bonds and ionic interactions on crosslink density determination)

Eqs. (10) and (11) apply to hydrogel systems based on single polymer. A mathematical model for predicting the crosslink density of complex ionically crosslinked hydrogel systems based on a mixture of different polymers was developed using Eqs. (10) and (11) simultaneously. Therefore, Eq. (12) is a general mathematical model for determining the crosslink density of all hydrogel systems as a function of the type and concentration of polymers and crosslinking agents:

$$\rho_x = \sum_{i=0}^{n} \frac{\overline{N_{ion,i}}\, m_{p,i}\, X_{ion,i}}{2} e^{-\frac{a_{ion}}{x}} + \sum_{i=0}^{n} \frac{\overline{N_{hyd,i}}\,\left(m_{p,i} - m_{p0,i}\right) X_{hyd,i}}{2} a_{hyd} \tag{12}$$

where i and n are particular polymer and the number of all polymers in the hydrogel system, respectively, and $X_{ion,i}$ is the mass fraction of polymer i in the hydrogel system. All other terms in the model are the same as described under Eqs. (10) and (11) for a particular polymer i in the hydrogel system. In the end, a_{hyd} is constant for all systems with hydrogen interactions, and a_{ion} is a property of the ionic crosslinking agent in the hydrogel.

3.2. Rheological characterization of hydrogels and verification of developed mathematical model based on polymer-polymer interactions in hydrogel network

The mechanical spectra are concentrated on the frequency dependence of the storage (G') and loss (G'') moduli on the angular frequency, with the lines showing the Maxwell-Wiechert model predictions (Eqs. (1) and (2)). The shear moduli G (Table S2) were determined by the sum of Maxwell's elastic elements G_e and G_k (Eq. (3)) (in the same way as in (Kopač et al., 2020)). Moreover, these data are used to determine the crosslink density (Eq. (7)) and the average mesh size (Eq. (8)) of the hydrogel network. In parallel with the model verification, the influence of the polymer-polymer interaction effect on the viscoelastic behavior, the crosslink density and the mesh size of the hydrogel network is investigated in detail.

The various hydrogel systems were prepared at different concentration (1–3 wt%) of the single polymer. This is the range where the most significant changes in the structure of the hydrogel network occur, while at polymer concentration up to 1 wt%, the hydrogels are weaker or do not even express the typical 3D structure (Lapasin et al., 2017; Šebenik et al., 2020). Ionic crosslinked hydrogels were further investigated by adding a calcium ion solution at a maximum concentration of 2 wt%. Under this condition, it was found that almost all carboxyl groups of TOCNF are involved in the crosslinking process, so that a higher concentration of crosslinking agent solution would not (noticeably) affect the rheological properties of the hydrogels (Kopač et al., 2020; Kopač et al., 2021).

In order to comprehensively verify the proposed model, complex hydrogel systems were prepared, which can be usefully classified into four groups: (i) equivalent blends of the constituent biopolymers with different concentrations (1–3 wt%) without the addition of crosslinking agent are shown in Fig. 2 (concentration dependence), (ii) blends of 2 wt % constituent biopolymers in different weight ratios (from 90 to 10 wt% of each biopolymer - presented in different colors) are illustrated in Fig. 3 (fraction dependence), (iii) the blends from (ii) were crosslinked by spraying a 2 wt% solution of calcium ions in the same volume ratio to the mixtures, where Fig. 4 shows the results of a constant crosslinker, and (iv) equivalent blends of constituent biopolymers crosslinked by spraying a solution of calcium ions (colors represent different concentrations of calcium ion solution ranging from 0.17 to 2 wt%) in the same volume ratio to the mixtures are shown in Fig. 5 (different crosslinker). In addition to the complex hydrogel mixtures, the results of the constituent biopolymers are also shown in Fig. 1. The detailed rheological characterization of the single constituent biopolymer dispersions (TOCNF, SCLG and LAP) can be found in the literature (Lapasin et al., 2017; Šebenik et al., 2019, 2020).

3.2.1. Single polymer hydrogel

Single polymer hydrogels based on the constituent biopolymers (TOCNF, ALG and SCLG) and LAP (clay) exhibit a pronounced viscoelastic behavior. For reference, 2 wt% of TOCNF, SCLG and LAP without the addition of crosslinking agent (ALG is reasonably not included) are presented showing increased viscoelastic behavior (G' and G'') from TOCNF, over SCLG to LAP hydrogel samples (Fig. 1). Accordingly, the TOCNF forms the hydrogel structure due to the presence of three hydroxyl groups on each β-(1–4)-glucopyranosyl unit (Klemm et al., 2011; L. Liang et al., 2020), which contributes to the formation of intra- and

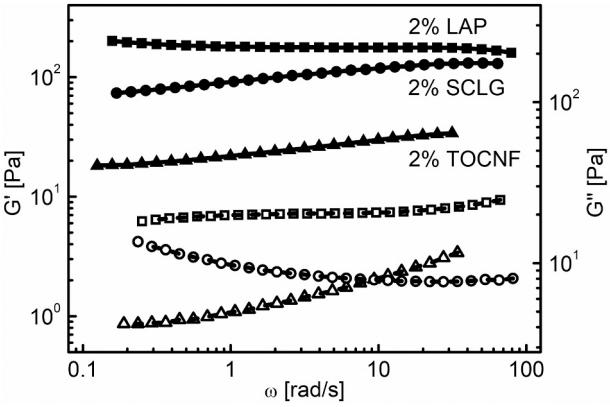

Fig. 1. Mechanical spectra of single polymer hydrogel. The triangles, circles and squares represent the 2 wt% of TOCNF, SCLG and LAP hydrogel, respectively. Storage modulus G' (filled symbols) and loss modulus G'' (empty symbols) are presented.

intermolecular hydrogen bonds (Lin & Dufresne, 2014) that play a pivotal role in the physical and chemical properties of cellulose fibers (Lundahl et al., 2018). Secondly, SCLG is used as a thickening and suspending agent and is suitable for the formulation of hydrogel matrices for the sustained release of bioactive molecules (Lapasin et al., 2017; Paolicelli et al., 2017). The structure consists of β-D-glucopyranosyl units (1,3) linked in the main chain, with three triplex chains holding hydrogen bonds to each other in the center of the triplex, reflecting in the higher mechanical properties values as in the case of TOCNF. A single β-D-glucopyranosyl unit (1,6) linked to the main chain prevents intermolecular aggregation and polymer precipitation (Tommasina Coviello et al., 2005; Lapasin et al., 2017). The triplex conformation is characterized by a high rigidity which is responsible for the peculiar properties of aqueous SCLG solutions in a wide pH range and also at relatively high temperatures (Lapasin et al., 2017). The intra- and intermolecular hydrogen bonds between the main chains of SCLG lead to the formation of stable rigid triple helices in aqueous solutions (Nazmabadi et al., 2020). On the other hand, the mechanical properties of LAP are even higher than of TOCNF and SCLG. The synthetic hectorite LAP single layer nanoparticles in the form of a rigid, disk-shaped crystals are usually used as a rheological modifier. LAP disks dispersed and swollen in aqueous media possess a permanent negative charge on the faces as a result of dissociation of Na^+ ions and diffusion from the stacks. Due to the protonation of hydroxyl groups, the edge of the particles is slightly positively charged instead (Park et al., 2020; Šebenik et al., 2020). The mechanism of formation of the extended thixotropic LAP gel structure involves the reaction of LAP particles with hydroxide ions in water, which causes the dissolution of phosphate ions. It is followed by forming interactions between LAP particles while the sodium ions diffuse towards the surfaces within the galleries, allowing the formation of gel structure (Afghah et al., 2020). The addition of Laponite to biopolymer weak gel could contribute to faster development of final gel properties (aging), better control of release kinetics and also improve the mechanical properties of the matrix (Šebenik et al., 2020). According to literature (Lapasin et al., 2017), the LAP dispersion of less than 0.75 wt% has the properties of a Newtonian fluid or shows no viscoelastic character, therefore the blending would have only a dilution effect and no synergistic interaction between LAP nanoparticles and biopolymer network. Furthermore, the storage time has an even greater effect on sharp sol-gel transition than clay concentration (Šebenik et al., 2020). To obtain stable rheological properties, 2 wt% LAP hydrogels were prepared and stored at 4.2 °C for 15 days (as reported in (Šebenik et al., 2020)), since aging of SCLG and TOCNF hydrogels affects the rheological properties. Although aging is essential to reach final hydrogel properties, a more significant contribution to the hydrogel properties

has biopolymer concentration. At a concentration of 1–3 wt% SCLG and TOCNF, the prepared hydrogels (without crosslinker) exhibit a stable network structure when stored for 15 days (already reported in (Lapasin et al., 2017; Šebenik et al., 2019)). On the opposite, ALG, a water-soluble linear copolymer composed of (1 → 4)-linked α-L-guluronic (G) and β-D-mannuronic (M) residues of varying sequence, only forms a hydrogel structure (high mechanical properties) in the presence of divalent cations (e.g. Ca^{2+}) (Hecht & Srebnik, 2016).

3.2.2. Concentration dependence hydrogel systems

SCLG/TOCNF hydrogel systems were prepared to investigate the importance and influence of the concentration of the biopolymer on the final mechanical properties of the hydrogels. The samples were prepared without the crosslinking agent by blending various (1–3 wt%) concentrations of SCLG and TOCNF in equal weight ratios (Fig. 2) and subjected to aging until the final properties were obtained. Both the elastic (*G'*) and the viscous (*G"*) moduli increase with increasing biopolymer concentration, indicating the existence of invisibly small clusters with significant swelling ability in water. The clusters are formed during the storage process (aging) of the prepared hydrogels when predominantly hydrogen, van der Waals and electrostatic repulsive forces begin to intertwine in the SCLG and TOCNF network structure. During the aging process, the clusters increase in size, reducing their distance from each other and further enhancing the noncovalent interactions among them. After a certain time, the growth of the clusters slows down reaching the final properties of the hydrogel structure (approx. 2 weeks (Šebenik et al., 2019)). TOCNF polymers with modified carboxyl groups on the surface are an exception, where clusters are also formed during the ionic or covalent crosslinking process. As it can be seen in Fig. 2, TOCNF concentration has a less important influence on the mechanical spectrum. Furthermore, the reduction of both *G'* and *G"* clearly displays a weaker hydrogel structure at low biopolymer concentration. This is also confirmed by the lower shear moduli *G* (see Table S2) at lower biopolymer concentration. As shear modulus is directly proportional to the crosslink density in the hydrogel network (Fanesi et al., 2018; Kopač et al., 2020), this is an additional confirmation of the hydrogel network weakening.

3.2.3. Fraction dependence hydrogel systems

Next, the effect of the mass fraction of different biopolymers on the mechanical properties of hydrogel mixtures was studied in the case of blending 2 wt% hydrogels of TOCNF, SCLG, LAP and ALG (see single polymer hydrogel properties from Section 3.1. as reference). The mixtures were prepared in mass fractions of both biopolymers from 0.9 to 0.1 (Fig. 3). Accordingly, 2 wt% SCLG/TOCNF (Fig. 3A) and SCLG/ALG (Fig. 3C) blends implies the *G'* and *G"* increase, whereas the addition of SCLG mainly affects the elastic properties of the hydrogel due to the high concentration of hydroxyl groups on the surface (4.2 mmol/g) forming hydrogen interactions. That is confirmed by changing the SCLG with LAP (Fig. 3B), when, at the low LAP concentration, the hydrogel structure is not developed (green circles) (LAP establishes electrostatic interactions, but ALG does not participate in crosslinking due to high water solubility). The mechanical spectrum reports an increase in *G'* and *G"* moduli at a higher mass fraction of SCLG. The mechanical properties of the SCLG/TOCNF are more similar to the properties of the single SCLG hydrogel, but at the same time, the *G'* and *G"* increase with the angular frequency and along these lines express weakness of the mechanical structures of the hydrogels, which is more a characteristic of the single TOCNF hydrogel (see Fig. 1). On the other hand, the effect of ALG in hydrogel systems without crosslinking agent addition is reflected in weaker mechanical structures, since the presence of ALG in the mixture does not lead to additional interactions between polymers due to its high water solubility.

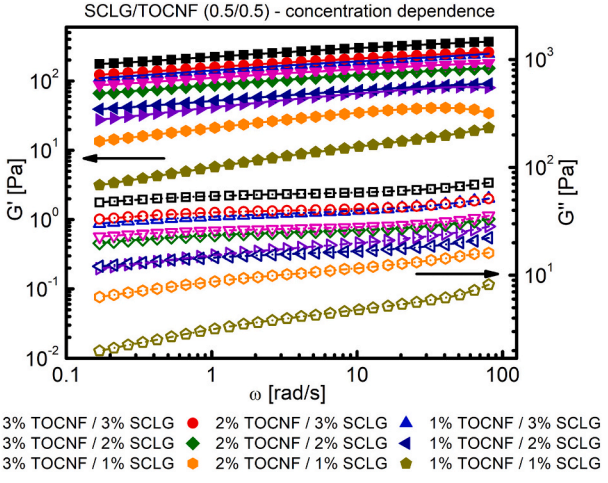

Fig. 2. Mechanical spectra of SCLG/TOCNF hydrogel blends without crosslinking agent in equal weight ratio. The different shape of symbols represents the various concentrations of biopolymer in single polymer hydrogel preparation. Storage modulus *G'* (filled symbols) and loss modulus *G"* (empty symbols) are presented with the addition of model fit Eq. (1) and (2), respectively.

3.2.4. Fraction dependence of biopolymer blends on complex equally crosslinked hydrogel systems

Biopolymer blends from Section 3.3 were additionally crosslinked with 2 wt% calcium ions solution to establish crosslinked hydrogel systems. The mechanical properties of such systems are shown in Fig. 4. and depend on the crosslink density resulting from a number of ionic, hydrogen and other van der Waals interactions. Therefore, *G'* and *G"*, and, consequently, the shear moduli *G*, increase with the increasing mass fraction of TOCNF or ALG in hydrogel systems (higher carboxylate level, more ionic interactions during crosslinking and higher crosslink density). Anionic carboxyl groups give the hydrogel pH responsivity (Way et al., 2012) (alkaline release trigger) and also allow the control of crosslink density (Lin et al., 2012), mesh size (Patiño-Masó et al., 2019) and flow properties (Kopač et al., 2020) by crosslinking via divalent ions (Curvello & Garnier, 2020; Xu et al., 2019). The mechanical spectrum reports a nearly independent influence of angular frequency on *G'* and *G"* for all systems, which confirms the very stable hydrogel network structure of ionically crosslinked hydrogel systems (the presence of strong ionic interactions (compared to hydrogen interactions) significantly increases the shear moduli of crosslinked SCLG/TOCNF hydrogels).

The rheological properties of non-crosslinked LAP/TOCNF are presented in the literature (Šebenik et al., 2020), although, in this study, the focus is on the more complex hydrogel structure of ionically crosslinked TOCNF biopolymer chains. The effects of hydrogen and ionic interactions are predominating and fraction dependent on crosslinked SCLG/TOCNF systems (Fig. 4A). Differently, in the case of crosslinked LAP/TOCNF systems (Fig. 4B), the effect of hydrogen bonds is lower in exchange for electrostatic interactions between LAP nanodisks (positively charged edges of particles) and TOCNF fibrils (anionic side groups). The clay particles of LAP and its aggregated forms are deposited between the polymer chains of TOCNF, which additionally connect the polymer nanofibers and strengthens the mechanical properties of hydrogel systems (Lapasin et al., 2017; Šebenik et al., 2020). The effect of electrostatic interaction between LAP and TOCNF is evident as the *G'* and *G"* values are significantly higher (Fig. 4B) than in SCLG (nonionic polymer)/TOCNF based system (Fig. 4A). At higher TOCNF content, the increase in shear modulus is slowed down due to the high crosslink density of TOCNF chains, preventing LAP nanoparticles to develop an extended aggregation structure comparable to the structure of a single LAP system (Lapasin et al., 2017). Similar conclusions can be reached in the case of hydrogel systems where TOCNF is replaced with ALG (Fig. 4C and D). In this case, even more pronounced mechanical properties are evident due to the higher concentration of carboxyl groups on the ALG

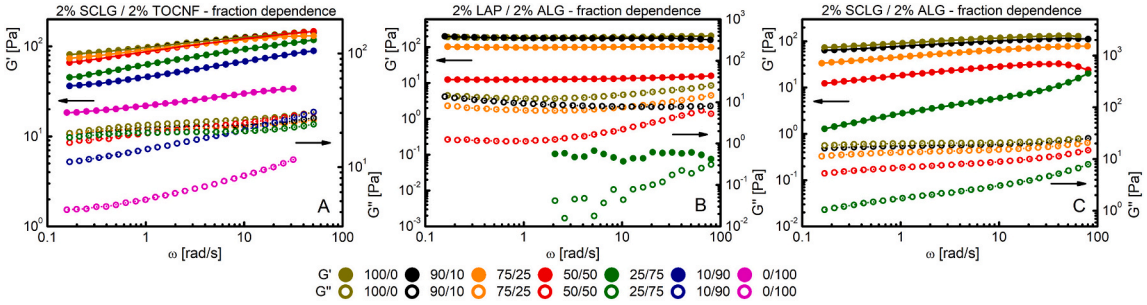

Fig. 3. Mechanical spectra of 2 wt% SCLG, TOCNF, ALG and LAP hydrogel blends in different weight ratio without crosslinking agent. The colors of the circles represent the weight ratios of the constituent 2 wt% single polymer hydrogels. Storage modulus *G'* (filled symbols) and loss modulus *G"* (empty symbols) are presented. The *G'* and *G"* are not reported for samples where x/ALG = 0/100 or 10/90 due to blend solution behavior.

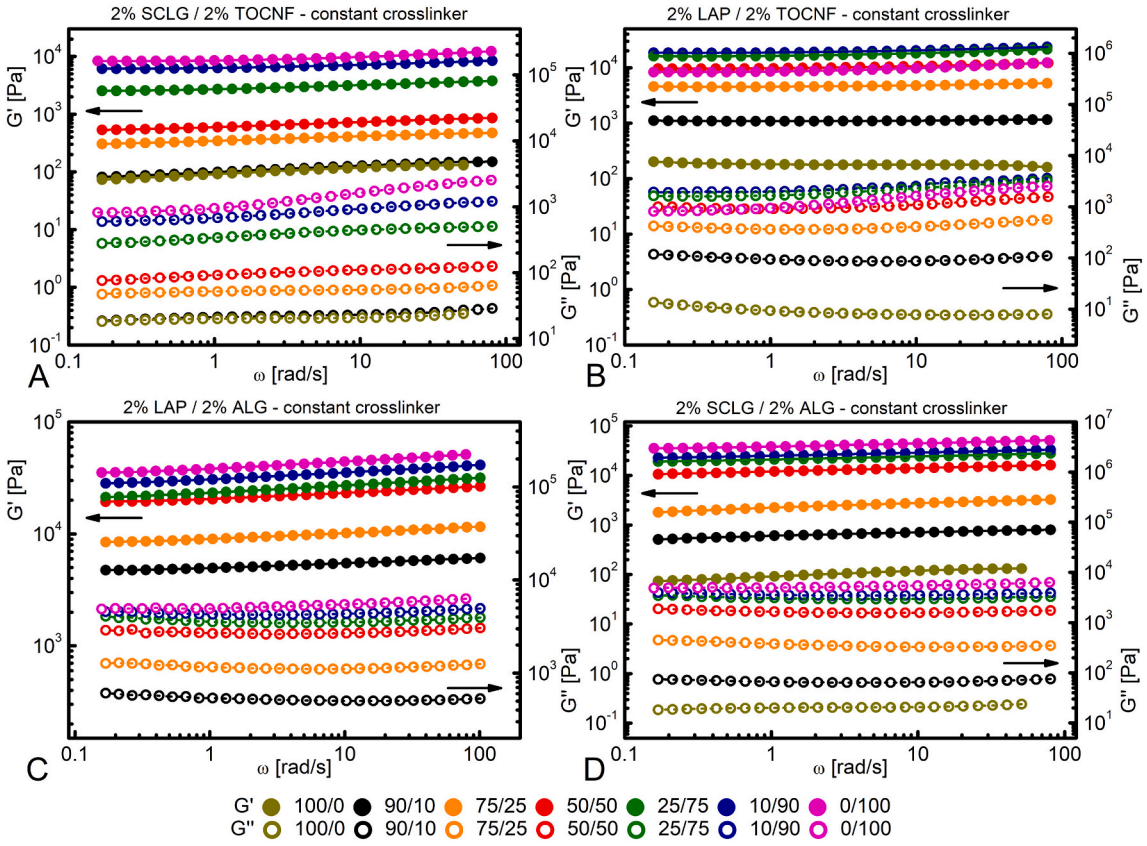

Fig. 4. Mechanical spectra of crosslinked (constant – 2 wt% addition of crosslinking agent solution) 2 wt% SCLG, TOCNF, ALG and LAP hydrogel blends. The colors of the circles represent the weight ratios of the constituent 2 wt% single polymer hydrogels. Storage modulus *G'* (filled symbols) and loss modulus *G"* (empty symbols) are presented.

surface (2.6 mmol/g) than on TOCNF (1.2 mmol/g). On the other hand, as evident from Fig. 3B, ALG does not form hydrogen or electrostatic (with LAP particles) interactions inside polymer network unlike TOCNF (2.8 mmol/g of hydroxyl groups). By comparing Fig. 4C and D, LAP and SCLG have almost no effect on the storage modulus when blended with ALG (the reduction of *G'* and *G"* is a consequence of the lower ALG content–lower carboxylate level). The predominant effect of stronger ionic interactions is presented in ALG containing hydrogels (the highest *G'* and *G"* values in Fig. 4). At a lower fraction of ALG (below 0.25), the effect of electrostatic interaction between LAP and calcium alginate (Fig. 4C) can be detected which was not present in non–crosslinked LAP/ALG samples (Fig. 3B).

3.2.5. *Effect of crosslinking agent concentration on complex hydrogel systems*

To study the effect of crosslinking agent concentration on the mechanical properties of hydrogel systems, biopolymers were blended in the 0.5/0.5 weight ratio (see Section 3.2) and additionally crosslinked with different concentrations of calcium ion solution (0.17–2 wt%) in the same way as explained in Section 3.2.4. Also, the ionic bonds between the TOCNF or ALG polymer chains formed during the crosslinking process with calcium ions (Curvello & Garnier, 2020) are predominant over other interactions. For that reason, there are no major differences in trend of mechanical properties between the SCLG/TOCNF and LAP/TOCNF or SCLG/ALG and LAP/ALG hydrogel systems (Fig. 5). However, the major effect of the crosslinking agent on the mechanical properties of prepared hydrogel samples is evident. The higher the crosslinking agent concentration, the more ionic interactions are formed between

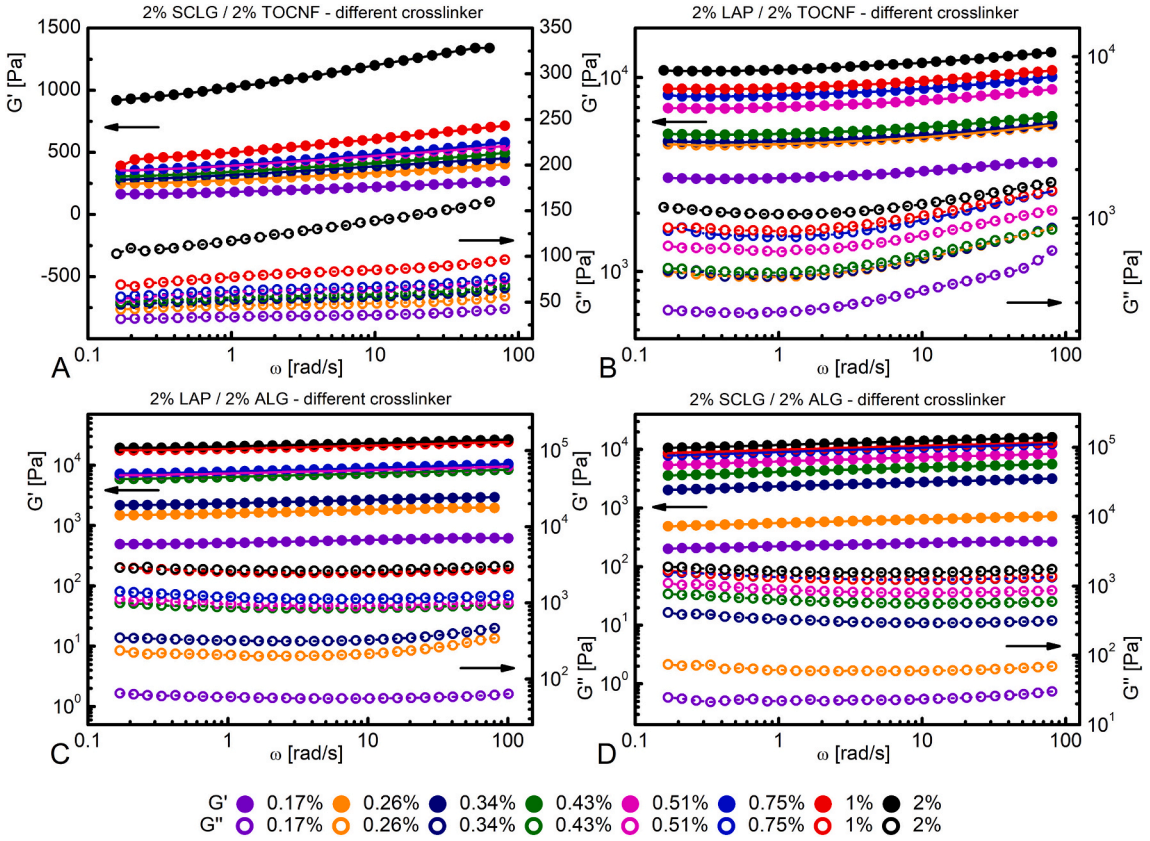

Fig. 5. Mechanical spectra of crosslinked 2 wt% SCLG, TOCNF, ALG and LAP hydrogel blend systems in equivalent weight ratio. The symbols represent the concentration of the added crosslinking agent solution. Storage modulus *G'* (filled symbols) and loss modulus *G"* (empty symbols) are presented.

ALG or TOCNF polymer chains and, consequently, the higher *G'* and *G"*. Overall, the *G'* and *G"* values of differently crosslinked hydrogels (Fig. 5) are close to those in Section 3.2.4. (constant crosslinker) (Fig. 4) (predominant effect of ionic interactions). The SCLG/TOCNF system (Fig. 5A) differs a little bit from the other mixtures as the effect of crosslinker increase is less evident, at least up to the maximum concentration explored (2%). As it will be detailed in Section 3.3, this could be due to a competition between hydrogen bonds, forming between SCLG and TOCNF, and ionic bonds, mediated by Ca^{+2}, forming between TOCNF chains. Only when Ca^{+2} concentration exceeds 1%, we can see the clear effect of ionic TOCNF-TOCNF interactions that reflects in a clear increase of *G'*.

3.2.6. *Verification of developed Eq. (12) for crosslink density calculation of (complex) hydrogels*

After the rheological characterization of different hydrogel systems, the experimental data of rheological measurements were compared to theoretically predicted crosslinking densities of the hydrogels with respect to polymer-polymer interactions (Fig. 6). The agreement between the experimental and calculated values is presented by the parity plot added in the Supplementary material (Figs. S1–S4). The experimentally determined crosslink density was resolved using the shear modulus in Eq. (7) and used as a verification for proposed Eq. (12). In addition, please find models for a_{ion} and a_{hyd} determination in supplementary material (Eqs. C.1–C.3). In Fig. 6A, an excellent match between model prediction and experimental data can be observed. TOCNF, SCLG and LAP hydrogels are formed in water due to hydrogen interactions established between polymer-polymer chains creating a network, which enables water to diffuse (due to hydrophilicity) in the internal structure. In this case, where the effect of hydrogen interaction on crosslink density is predominant, the approximation (Eq. (10)) of Eq. (12) can be used. Additionally, the proposed model predicts the final crosslink density of gels when mechanical properties are stable and are not time–dependent (after the aging in the case of non-crosslinked samples).

The fraction dependence on hydrogel systems based on mixing single polymer hydrogels is presented in Fig. 6B. In this case, the crosslink density can be calculated in the same way as before taking into account the mass fraction of polymer in the mixture. As is evident in Fig. 6A, the ALG does not form hydrogen interactions due to good solubility in water (discussed in detail in Sections 3.2.1 and 3.2.3). Furthermore, the crosslink density of ionically crosslinked hydrogels with different mass fractions of consistent polymers is presented in Fig. 6C and D. The combined effect of hydrogen and ionic interactions on crosslink density was calculated by using Eq. (12). However, as previously reported, the ionic interactions are much stronger than hydrogen interactions, hence in this case also the approximation in the form Eq. (11) can be used. Not surprisingly, as also noted in the previous section (Section 3.2.5), the SCLG-TOCNF system displays an anomalous behavior, at least with respect to model prediction. Again, the reason for this evidence should be attributed to the competition between TOCNF-TOCNF Ca^{+2} mediated ionic interactions and TOCNF-SCLG hydrogen bonds. Indeed, Fig. 6B makes clear that in SCLG/TOCNF system, the effect of hydrogen bonding is considerable, at least with respect to LAP/ALG and SCLG/ALG mixtures that are characterized by lower crosslink densities. This is, probably, the reason why our model underestimates (see the line over symbols not under) the experimental data of Fig. 6C and D. The LF-NMR characterization presented in Section 3.3 also will confirms this interpretation.

Hydrogel networks are characterized by the interweaving of hydrophilic chains of constituent polymers, which are interconnected by various interactions (ionic, hydrogen, other electrostatic forces and covalent bonds) that increase the crosslink density and thus form a characteristic three-dimensional structure of hydrogels (Mahinroosta et al., 2018). The predominant role is played by the type and number of

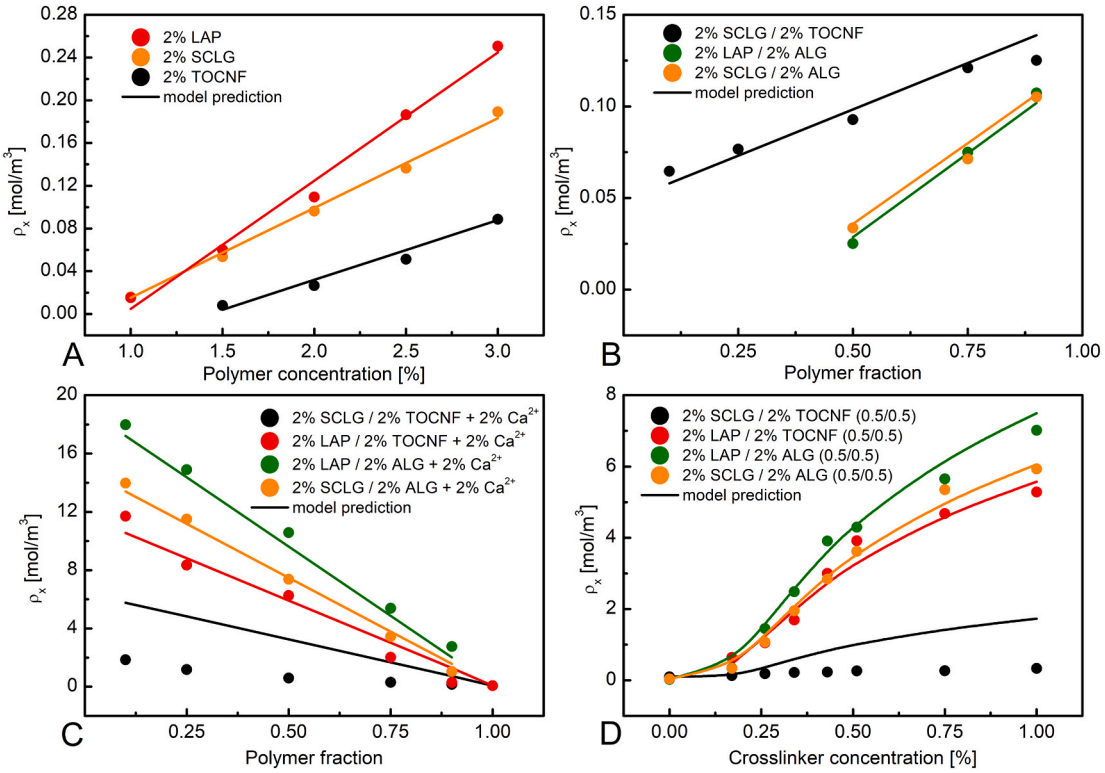

Fig. 6. Crosslink density of single polymer hydrogel without crosslinking agent (A) (refers to the data shown in Fig. 2), fraction dependence on hydrogel systems without crosslinking agent (B) (refers to the data shown in Fig. 3), fraction dependence on equally crosslinked hydrogel systems (C) (refers to the data shown in Fig. 4) and effect of crosslinking agent concentration on complex hydrogel systems (D) (refers to the data shown in Fig. 5). The circles represent the experimental values (please find Table S2 in Supporting material) adopted by rheological measurements (Figs. 2–5) and lines represent the theoretical values calculated by new developed Eq. (12) (see also parity plot (Figs. S1–S4) supplemented in Supplementary material).

polymer-polymer interactions that significantly affect hydrogel network characteristics, rheological (mechanical) properties, crosslink density, and also the release rate in the case of drug delivery systems. Following that, the linear dependence of polymer concentration and polymer fraction of polymers in hydrogel blends on crosslink density is evident in Figs. 6A–C due to the various concentration of substituent groups (carboxyl and hydroxyl groups) with a good model prediction. Hydrogen bonds predominate in SCLG and TOCNF systems without the addition of a crosslinker (Fig. 6A and B). In such systems, the contribution of hydrogen interactions to the hydrogel network depends on the concentration of the polymer or the mass fractions between the polymers in the hydrogel blends (Fig. 6B). On the other hand, the distance between polymer chains in the hydrogel is spaced apart from each other so that a hydrogen interaction cannot be created between all the hydroxyl groups available. According to the literature, the typical length of a hydrogen bond in water are ≈200–350 pm (Sheu et al., 2003). Polymer chains are closest to each other at crosslink points, where these links may take the form of ionic bonds (or covalent bonds in the case of chemical crosslinking). Obviously, longer distances between the polymer chains do not allow the formation of hydrogen bonds. Hydroxyl groups that do not form hydrogen bonds, due to their hydrophilicity allow water to diffuse into the hydrogel network (swelling) (Hoare & Kohane, 2008). Even more, in the case of low carboxylate level, the hydrogen bonds can be predominated over few ionic interactions (Fig. 6D). Finally, the shape of particles is not negligible in the formation of hydrogen bonds, as SCLG has a larger surface area than TOCNF fibers.

The exponential effect of crosslinking agent concentration on crosslink density of hydrogels is illustrated in Fig. 6D. In the low crosslinking agent concentration range (up to 0.51 wt%), the effect on crosslink density is linear due to the high concentration of free carboxyl groups in comparison with calcium ion concentration. At exalted crosslinking concentrations (above 1 wt%), the number of free carboxyl groups decreases reaching the limit for each calcium ion to generate crosslink points. The comparison of the results between systems with and without crosslinker proves the predominance of ionic bonds over other interactions (Section 3.2.5), regardless of the amount of the ionic interactions. For example, on the surface of TOCNF the carboxylate level is 1.2 mmol/g (Kopač et al., 2021) and the available quantity of hydroxyl groups is 2.8 mmol/g (Ho et al., 2011). Theoretically, it is possible that more than two times more hydrogen bonds are formed between TOCNF polymer chains than ionic ones. On the other hand, SCLG/TOCNF systems contain even more hydroxyl groups due to the addition of SCLG (4.2 mmol/g hydroxyl groups on the surface). However, ionic bonds (up to 2000 kJ/mol (Mehandzhiyski et al., 2015)) formed are stronger than hydrogen (≈20 kJ/mol (Sheu et al., 2003)), which is why they have a predominant effect despite the numerical domination of hydrogen bonds. Therefore, the concentration of the crosslinker and the polymer containing functional groups susceptible to ionic crosslinking is crucial for the controlled design of ionically crosslinked hydrogels with the desired properties.

Not to mention only ionic and hydrogen interactions, other electrostatic interactions are formed between LAP particles having negative and positive charges on the surface (Ruzicka & Zaccarelli, 2011; Šebenik et al., 2020) and carboxyl groups (negative charge) on TOCNF or ALG chains that do not participate in ionic crosslinking (higher crosslinking agent concentration, lower content of free carboxyl groups and consequently reducing the number of electrostatic interactions). The content of electrostatic interactions is consequently controlled by the concentration of polymers with ionic functional groups or the concentration of particles with different charges (e.g. LAP), as well as by the concentration of the crosslinker. Therefore, electrostatic interactions have a significant effect on the mechanical properties and crosslink density of

hydrogels with a low concentration of ionic crosslinker (up to 0.34 wt%) as well discussed in Section 3.2.5. At higher crosslinking agent concentrations, less free ionic functional groups are present on the surface of the hydrogel, so the effect of electrostatic interactions is less obvious (but still not insignificant) (see Fig. 4).

To conclude, the developed Eq. (12) based on polymer-polymer interaction in hydrogel network enables to satisfactorily calculate the crosslink density of gels. The model was verified based on complex hydrogel systems which are formed due to the predominant effect of ionic and hydrogen interaction. The presented study is based on biopolymer in absence of toxic chemical crosslinking agents having a great potential to be used for hydrogel design in different biomedical and biopharmaceutical applications. Furthermore, the principle of crosslink density calculation based on chemically crosslinked hydrogel should be the same, with the determination of crosslinking agent functionality affinity (a_{chem}) in the same way as presented in our previous article (Kopač et al., 2020).

3.3. LF-NMR characterization of hydrogel networks

LF-NMR measurements were performed as an interpretation and validity supplement to the developed model equation Eq. (12), which predicts the crosslink density of hydrogels based on polymer-polymer interactions. LF-NMR characterization of gels relies on the effect of solid surfaces (polymer chains, etc.) on the magnetic relaxation process of water hydrogens subjected to a sudden variation of an external magnetic field (Abrami et al., 2018). Indeed, different spatial organizations of polymeric chains imply different values of the ratio between the solid surface (S) in contact with water molecules present in the system (hydrogel) volume (V). This, in turn, reflects in a variation of the mean relaxation time T_{2m} of water protons. In particular, the addition of a crosslinker or, simply, the spontaneous formation of physical interactions (such as hydrogen bonds), obliges chains to modify their relative position in the gel volume so that, for example, original chains bundles can be disrupted to give rise to a different three-dimensional organization (Abrami et al., 2018; Fanesi et al., 2018). This is the reason why, typically, the sol-gel transition implies the reduction of T_{2m} (Abrami et al., 2019).

From Table S2 it immediately appears that the 2% ALG system is characterized by a high relaxation time ≈1800 ms (free water at 25 °C $T_2 = 2500$ ms) and only one component of the relaxation spectrum (T_{21}), this witnessing that we are dealing with a homogeneous solution. On the contrary, 2% TOCNF and 2% SCLG systems are characterized by lower T_{2m} and this supports the idea that hydrogen bonds play an important role in the nano-structure organization of TOCNF-SCLG system that, indeed, is a gel as witnessed by Fig. 3A. While TOCNF presents almost one T_2 (homogeneous solution), 2% SCLG presents two T_{2i}, indicating the presence of an inhomogeneous system where rich polymer clusters are embedded in a continuous phase characterized by a lower polymer concentration. A clear difference existing among single polymer samples underlines that 2% SCLG is not a homogeneous solution and sampling can affect the measurement due to sample heterogeneity.

Fig. 7 reports the average relaxation times (black columns) of water protons, while the relaxation time distribution for each sample as a non-homogeneity indicator is given in Supplementary material (Figs. S5–S19). For reference, the theoretically calculated mesh size, calculated from Eq. (8), based on newly developed Eq. (12), and experimentally determined mesh size of hydrogels based on mechanical spectra results (the shear modulus from Eq. (3) were incorporated in Eq. (7) and (8)) are illustrated in Fig. 7 as green and red, respectively. Additionally, average relaxation times were fitted by Eq. (6) to determine M as the fitting parameter for the particular hydrogel system.

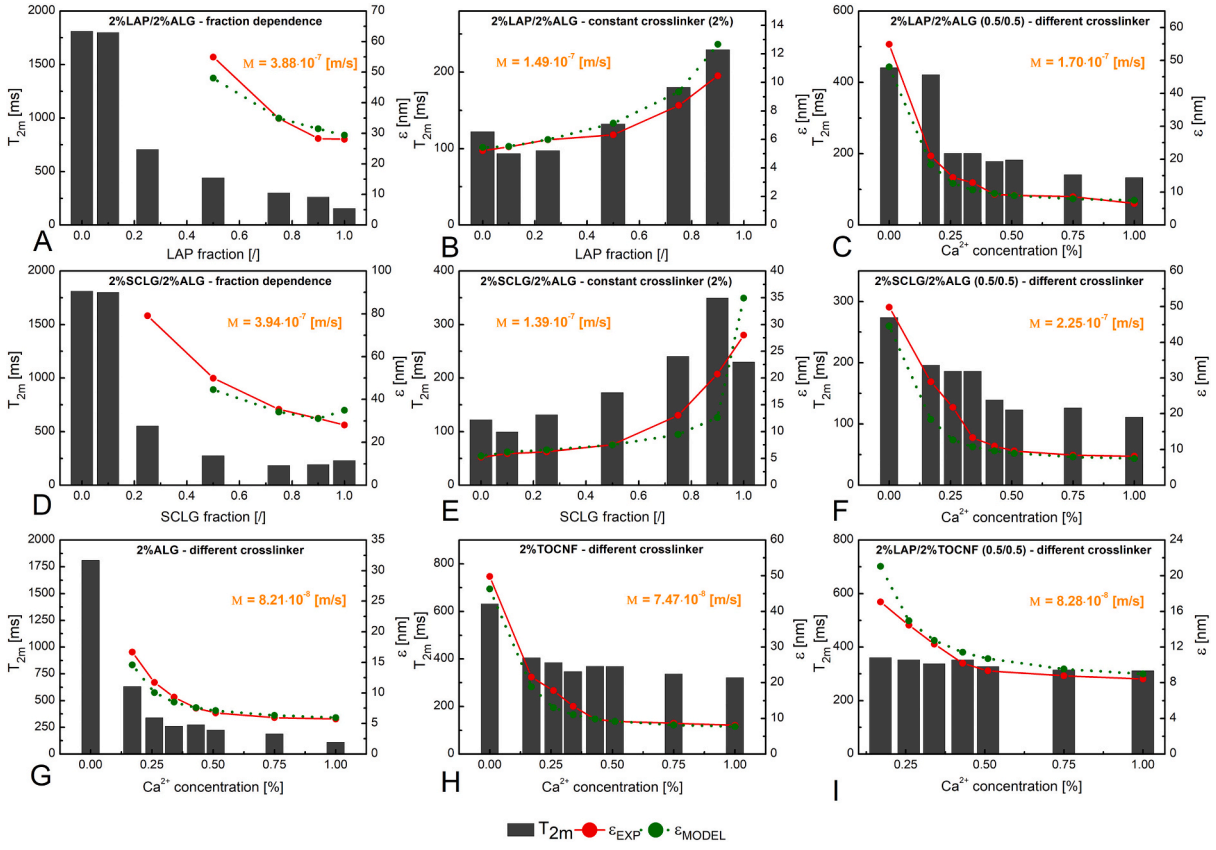

Fig. 7. LF-NMR characterization of hydrogel network. Columns represent the average relaxation time of water protons in different hydrogels, symbols represent the average mesh size of hydrogel determined by rheological measurements (red circles) and the new developed model in Eq. (12) (green circles). M is Eq. (6) fitting parameter known as relaxivity. Due to the display clarity, 2% Ca^{2+} is not shown in figures, but could be found in a numerical form in SI, Table S2.

Fitting parameter M is characteristic for each system allowing to determine the mesh size on the basis of relaxation times from LF-NMR analysis (Kirchhof et al., 2015; Maestri et al., 2017). Interestingly the M values found in this paper are similar to those found by Coviello and co-workers who dealt with similar hydrogels (Coviello et al., 2013).

The LAP-contained systems (Fig. 7A–C) appeared fragile and discontinuous. The LAP decreases enhanced sample heterogeneity as the number of T_{2i} increased (see LF-NMR distribution times–supplement to Fig. 7 and Fig. 8 in supplementary material). Moreover, in systems without the addition of Ca^{2+} (Fig. 7A and D), the increase of ALG fraction implied an increase of T_{2m}. Upon ALG fraction increase, samples moved from soft gel to viscous solution. Indeed, as shown in Fig. 7D, T_{2m} grew with SCLG fraction reduction from 90:10 to 25:75. However, it is worth to underline that all blends appeared very inhomogeneous.

Additionally, from Fig. 7C, F and G it is obvious that divalent ions provoked the well-known crosslinks among ALG chains (egg-box junctions) even at the lower Ca^{2+} addition. Ca^{2+} concentration increase (from 0.17% to 2%) implies improving the strength of interactions, gel homogeneity (only one T_{2i} was necessary to describe hydrogens relaxation) and T_{2m} reduction. It is important to remind that, in all systems involving the ionotropic gelation of alginate, the evaluation of T_{2m} has been performed without considering the first relaxation time (T_{21}) if its value was >1300 ms. Indeed, a so high relaxation time can be only associated to water that is out of the polymeric network. The presence of external water is due to well-known syneresis effect implying a slow, time dependent, hydrogel de-swelling resulting in an exudation of liquids. Both alginate molecular weight and elastic segment flexibility play an important role in determining the entity of this phenomenon (Drageta et al., 2001).

As the negatively charged ALG chains are prone to rapidly interact with divalent cations, it is not surprising that T_{2m} decreased with the increment of ALG fraction (Fig. 7B and E). This also means that the polymeric network is characterized by gradually smaller meshes (T_{22} reduces). For Ca^{2+} of 0.17%, the sample looks like a viscous solution and only one T_2 is necessary to describe system magnetic relaxation. From $Ca^{2+} \geq 0.26\%$, samples look like rigid disks. T_{2m} is characterized by an initial decrease followed by a plateau (Fig. 7C, F and G–I). This is probably due to the shielding action exerted by LAP or SCLG towards the ALG or TOCNF Ca^{2+} interaction. In conclusion, we can presume that the addition of Ca^{2+} implies not only an increase of the shear modulus G (as proved by rheology) but also an appreciable increase of the S/V ratio implying a reduction of T_{2m}. Thus, in contrast to what happens in the case of SCLG/TOCNF, the increase in matrix stiffness with Ca^{2+} results from an increase in crosslink density (Fig. 8).

While a good trend for the prediction of the crosslink density could be observed for most samples (Fig. 6), SCLG/TOCNF hydrogel systems clearly deviate from the crosslink density prediction of the developed model, as already discussed in Section 3.2.6. An appropriate explanation for the apparent incongruity can be explained by LF-NMR spectroscopy, which enabled us to gain an insight into the nanostructure of complex hydrogel systems constituted by (ionically crosslinked) mixture of different polymers (Fanesi et al., 2018). Fig. 8A shows that the increase of TOCNF concentration entailed in an increase of T_{2m} and a blend homogenization, as at a 10:90 ratio (in favour of TOCNF) only one relaxation time appears, which resembles the situation occurring at pure 2% TOCNF (Table S2). This evolution could suggest that TOCNF nano-fibrils presence hinders the formation of the complex and heterogeneous SCLG network via the establishment of hydrogen bonds between TOCNF nano-fibrils and SCLG triple helices. Thus, TOCNF would sequester part of the SCLG triples helices that, ultimately, would be no longer available for network building up, this resulting in a weaker and more homogeneous network. An inspection of Fig. 6B supports this interpretation as it reveals that the TOCNF-SCLG system gives rise to higher crosslink density with respect to LAP-ALG and SCLG-ALG mixture. Furthermore, these considerations are also corroborated by Fig. 8C showing that the addition of Ca^{2+} has little effect on the blend structure (system without addition of Ca^{2+} (0%)) as, regardless of Ca^{+2} concentration, T_{2m} is almost constant. In addition, the relative relaxation spectra are similar each other being characterized by a prevalent T_{22} (300–500 ms) with A_2 ranging from 80 to 100%, i.e., a spectrum not far from sample 0% distribution (see Table S2). The scarce effect of Ca^{2+} should be due to the hydrogen bonding interaction arising among SCLG triple helices and TOCNF nano-fibrils that are no longer so prone to establish Ca^{+2} mediated ionic bonds. In this light it is worth mentioning that, theoretically, it is possible that more than two times hydrogen bonds are formed between TOCNF polymer chains than ionic ones as above discussed. The same argumentations can explain the results of Fig. 8C where a good comparison between model predictions (Eq. (12)) and experimental data occurs only for pure systems (SCLG fraction equal to 1 or zero). The fact that the rheological analysis records a variation of the shear modulus (G) of Fig. 8B and C systems while LF-NMR returns almost similar magnetic relaxation spectra, could be explained by supposing that matrix stiffness should not be due to the increase of crosslink density (moles of crosslinking points per unit volume) but to the augmentation of polymeric chains stiffness due to their grouping revealed by LF-NMR (hydrogen bonds among SCLG and TOCNF). Ultimately, these considerations underline that rheology and LF-NMR can see different aspects of a polymeric network: rheology – crosslink density, LF-NMR – chains disposition.

Thus, the combined use of rheology and LF-NMR indicates two different mechanisms at the basis of the ALG and TOCNF based systems crosslinking upon Ca^{2+} addition. The increase of matrix stiffness due to Ca^{2+} addition should be due to the increase of crosslink density in the case of ALG based systems. On the contrary, the formation of stiffer braided polymeric chains should be the reason for the G increase in TOCNF based systems.

The inspection of Figs. 7 and 8 reveals that, sometimes, there is not a very good correlation between ε (determined by means of rheological measurements – Eq. (7) and (8)) and T_{2m}. The reason for this relies on the physical principles on which rheology and LF-NMR are based on. Indeed, while rheology is affected only by elastically active chains (i.e. those involved in crosslinks), LF-NMR (i.e. T_{2m}) is affected by the conformation assumed by chains regardless of their enrollment in crosslinks. Indeed, T_{2m} is proportional to ratio between solvent volume

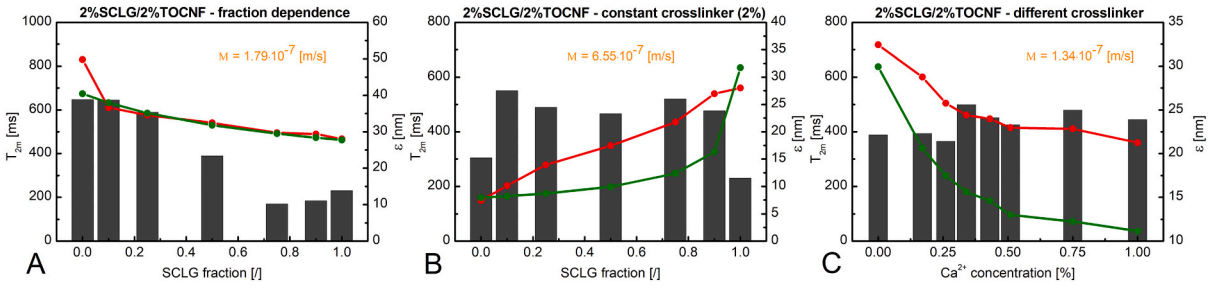

Fig. 8. LF-NMR characterization of hydrogel network. Columns represent average relaxation time of water protons in particular hydrogel network, symbols represent an average mesh size of hydrogel network determined by rheological measurements (red circles) and new developed model in Eq. (12) (green circles).

V (proportional to the number of solvent hydrogen) and the polymer chains surface S in contact with solvent molecules, proportional to the fraction of solvent hydrogen in strict contact with polymeric chains (the so-called bound solvent). This aspect can be clearly seen looking at Eq. (6) written in a less advanced form (Chui et al., 1995):

$$\left(\frac{1}{T_2}\right)m = \frac{1}{T_{2,H_2O}} + 2M\frac{S}{V} \quad \frac{V}{S} = \varepsilon\sqrt{\frac{1-0.58\varphi_p}{3\pi\varphi_p}} \quad \varepsilon = r_f\sqrt{3\pi\frac{1-0.58\varphi_p}{\varphi_p}} \tag{13}$$

An example of the different potentiality of rheology and T_{2m} in the characterization of hydrogels is reported by Marizza and co-workers (Marizza et al., 2016), who dealt with poly(*N*-vinyl-2-pyrrolidone) based hydrogels. Indeed, they noticed that the rheological and LF-NMR approach provided similar mesh size estimation only when the hydrogel shear modulus G was sufficiently large (140 Pa). On the contrary, for smaller G, rheology gave a larger estimation of the average mesh size. The explanation for this evidence consisted in the presence of dangling chains (or chains not directly involved in crosslinks) that, being bound to one end of the network, were elastically inactive and, thus, irrelevant for the determination of G and ε. Conversely, for LF-NMR (T_{2m}), both elastically active and inactive chains matter as both of them can affect the key parameter V/S. As the number of dangling chains can be roughly connected to the viscous properties of the gel (alias the loss or viscous modulus G''), Marizza concluded that dangling chains exert a smaller and smaller effect when G and G' (elastic or storage modulus) increase with respect to G''. In this condition, indeed, the rheological and LF-NMR approach provided similar ε estimation. A further support to this interpretation can be retrieved in the recent work of Descallar and co-workers (Descallar & Shingo Matsukawa, 2020) who studied the change of network structure in agarose gels by aging. In the last figure of the paper (Fig. 9), they provide a very interesting representation of the modification that the agarose network undergoes upon aging. As time goes on, polymeric chains get together to form a network characterized by the same crosslink density (or mesh size) but with thicker (and stronger) fibers. Although authors did not perform a rheological and T_{2m} characterization of their hydrogels, it is very probable that, upon aging, T_{2m} increases as S reduces due to chains grouping. At the same time, the shear modulus G should increase as the fibers section increases, despite the same crosslink density. These considerations suggest a possible strategy to get information on the gels network recurring to the combined use of rheology and LF-NMR. Indeed, when T_{2m} and ε show the same trend, we can conclude that a mesh size reduction/increase occurred as chains unbundle/bundle increased/reduced the number of chains available to establish crosslinks. On the contrary, when, for example, ε decreases and T_{2m} is almost constant, we can conclude that matrix stiffness increase is not really due to the crosslink density increase, but due to fibers stiffness increase (due to their bundling) as depicted in Fig. 9 of Wisniewska and coworkers (Wisniewska et al., 2018).

Another important consideration descending from Eq. (6) and (13) is represented by Eq. (14):

$$T_{2m} \propto \frac{1}{\left(\frac{1}{T_2}\right)_m} \propto \frac{\varepsilon\sqrt{\frac{1-0.58\varphi_p}{3\pi\varphi_p}}}{2\mathscr{M}} \tag{14}$$

Eq. (14) clearly shows that the relation between T_{2m} and ε depends on the polymer volume fraction φ_p and on relaxivity $\mathscr{M}$. Thus, even for constant φ_p, different $\mathscr{M}$ values reflect in different T_{2m} value at fixed ε. M represents the ratio between the thickness of the bound solvent (i.e., the thin solvent layer close to the polymeric chain surface that affects the magnetic relaxation of the bound solvent molecules) and its relaxation time (T_{2s}) (Chui et al., 1995). Thus, it is reasonable that different system compositions correspond to different M values as it happens in our systems (see the red values in Figs. 7 and 8). This is the reason why different T_{2m} values can be connected to the same mesh size or vice-versa.

It is also interesting to observe that despite the low polymer concentration of our systems, ε turns out to be quite small. This result can be explained on the basis of the Scherer theory (Scherer, 1994), approximated by Abrami and co-workers (Abrami et al., 2018), that establishes the relation between ε, φ_p and the polymeric chain radius r_f (each chain is assumed to be a long cylinder of radius r_f) as reported by the last equation of Eq. (13). In the case of alginate, for example, $r_f \approx 0.6$ nm (Amsden, 1998). Setting polymer concentration at 2%, this corresponding to $\varphi \approx 0.012$, the last equation of Eq. (13) provides $\varepsilon \approx 17$ nm, a value that is not far from what found in this paper. As polymer chains are very thin, it is possible getting small mesh size also in presence of a low polymer volume fraction. In addition, similar results were found by Wisniewska and coworkers (Wisniewska et al., 2018) who studied the structure of poly(*N*-isopropylacrylamide-*co*-acrylic acid) hydrogels. They found ε = 7–10 nm when polymer mass fraction ranges between 0.6 and 0.8%.

4. Conclusions

The new equation (Eq. 12) is proposed for theoretical determination of the crosslink density of hydrogels according to the concentration of polymer and crosslinking agents, the mass fraction between polymers and the concentration of substituent groups on the surface of polymers. The influence of different chemical bonds and their content on the final properties of the hydrogel was studied. The polymer-polymer interactions in hydrogel network which form the crosslink points was studied in detail by rheological (mechanical properties) and LF-NMR characterization (inhomogeneity of hydrogel network). In addition, to developed Eq. (12), the model to predict the average mesh size of hydrogel network based on LF-NMR measurements is enriched with the calculation of relaxivity M for particular hydrogel samples. Finally, the design of complex hydrogel systems according to the desired properties is possible, which can be further improved in future research by considering the contribution of covalent, van der Waals, heterotypic, hydrophobic, and other electrostatic interactions. The presented study could significantly shorten the research time and reduce the research cost in the future design of hydrogels with the desired properties.

CRediT authorship contribution statement

Tilen Kopač: Conceptualization, Methodology, Software, Validation, Formal analysis, Investigation, Writing – original draft, Visualization. **Michela Abrami:** Validation, Investigation. **Mario Grassi:** Software, Validation, Writing – review & editing, Supervision. **Aleš Ručigaj:** Software, Formal analysis, Data curation, Writing – review & editing, Visualization. **Matjaž Krajnc:** Resources, Supervision, Project administration, Funding acquisition.

Declaration of competing interest

The authors declared no conflicts of interest.

Acknowledgment

The authors acknowledge the financial support from the Slovenian Research Agency (research core funding no. P2-0191).

Appendix A. Flory-Rehner and Peppas-Merrill equation

Flory-Rehner equation:

$$-\left[ln(1-\nu_2)+\nu_2+\chi_1\nu_2^2\right]=\frac{V_1}{\bar{v}M_c}\left(1-\frac{2M_c}{M}\right)\left(\nu_2^{\frac{1}{3}}-\frac{\nu_2}{2}\right) \tag{A.1}$$

where ν_2 is the polymer volume fraction, χ_1 is the Flory solvent-polymer interaction parameter, V_1 is the molar volume of the solvent, $\bar{v}$ is the specific volume of the polymer, M is the primary molecular mass and M_c is the average molecular mass between crosslinks (Bruck, 1961).

Peppas-Merrill equation:

$$\frac{1}{\overline{M_c}}=\frac{2}{\overline{M_n}}-\frac{\left(\frac{\bar{v}}{V_1}\right)\left[ln\left(1-\nu_{2,s}\right)+\nu_{2,s}+\chi_1\nu_{2,s}^2\right]}{\nu_{2,r}\left[\left(\frac{\nu_{2,s}}{\nu_{2,r}}\right)^{\frac{1}{3}}-\frac{\nu_{2,s}}{2\nu_{2,r}}\right]} \tag{A.2}$$

where $\overline{M_n}$ is the number average molecular weight of a linear polymer (one formed without a crosslinking agent), $\nu_{2,s}$ and $\nu_{2,r}$ are polymer volume fraction in the swollen and relaxed state, respectively (Carr & Peppas, 2009).

The M_c determine the crosslink density ρ_x:

$$\rho_x=\frac{\rho}{M_c} \tag{A.3}$$

where the ρ is density of hydrogel.

Appendix B. Theoretical mathematical background of Eq. (6)

The origin of Eq. (6) derives from the "magnetization diffusion equation" proposed by Brownstein and Tarr (1979):

$$\frac{\partial\rho(\boldsymbol{r})}{\partial t}=\nabla\bullet(\mathrm{D}\bullet\nabla\rho(\boldsymbol{r}))-\theta\rho(\boldsymbol{r}) \tag{B.1}$$

where t is time, ρ is the magnetic moment density in the xy plane, $\boldsymbol{r}$ is the position vector, D is the water molecules self-diffusion coefficient (m^2/s), and θ is the volume sink strength density (s^{-1}). Due to the presence of paramagnetic impurities on surface (polymer chains) or hindrance in molecular tumbling close to surface (Chui et al., 1995), surface behaves as an absorber of magnetization so that relaxation is faster than in the bulk, i.e. far from solid surface. Consequently, the following boundary condition has to be accomplished:

$$(D\boldsymbol{n}\bullet\nabla\rho+\mu\rho)_S=0 \tag{B.2}$$

where $\boldsymbol{n}$ is the unit outward normal vector at the bounding surface S and μ is the surface sink strength density (m/s). The physical quantities μ and θ are connected to their respective, average, macroscopic, counterparts $\mathscr{M}$ (relaxivity) and Θ by:

$$M=\frac{\int\mu(r)dS}{S}\quad\Theta=\frac{\int\theta(r)dV}{V}\overset{\text{Chui et al.,1995}}{=}\frac{1}{T_{2,H_2O}} \tag{B.3}$$

where V is the volume of the water filling the polymeric network and T_{2H2O} is the spin-spin relaxation time of free (or bulk) water. Interestingly, $\mathscr{M}$ (m/s) is interpreted as the ratio between the thickness of the thin water layer surrounding the polymeric chain (the so-called surface or bound water) and the relaxation time of bound water (Chui et al., 1995).

The relation between the xy component of the magnetization (M_{xy}) and ρ is given by:

$$M_{xy}(t)=\int\rho(r,t)dV\quad M_{xy}(t=0)=\rho_0V \tag{B.4}$$

Eq. (B.1) integration on V, taking advantage of the divergence theorem, leads to (Chui et al., 1995):

$$\frac{dM}{dt}=-\mathscr{M}\iint\rho dS-\frac{1}{T_{2,H_2O}} \tag{B.5}$$

As Eq. (B.1) analytical solution reads (Chui et al., 1995):

$$M(t)=\sum_{i=1}^{\infty}I_ie^{\left(-\frac{t}{T_{2i}}\right)} \tag{B.6}$$

It is easy to verify that:

$$\frac{dM(t=0)}{dt}=-\sum_{i=1}^{\infty}\frac{I_i}{T_{2i}} \tag{B.7}$$

Remembering that $\rho(0)=M(0)/V$, for $t=0$, Eq. (B.5) can be written as:

$$-\frac{dM(t=0)/dt}{M(t=0)} = \sum_{i=1}^{\infty}\frac{I_i}{T_{2i}} = \left(\frac{1}{T_2}\right)_m = \frac{S}{V}\mathscr{M} + \frac{1}{T_{2,H_2O}} \tag{B.8}$$

Eq. (B.8) is nothing more than our Eq. (6).

Due to unavoidable magnetic field inhomogeneity, an additional term has to be considered on the right hand side of Eq. (B.8) when referring to the spin-spin relaxation time T_2 (this term disappears when dealing with the spin-lattice relaxation time T_1 (Coates et al., 1999)):

$$\frac{1}{T_{2D}} = \frac{D}{12}(\gamma\Delta G\tau)^2 \tag{B.9}$$

where γ (=4.26 × 10^7 Hz/T) is the gyromagnetic ratio for 1H and t (=0.25 ms) is the echo time, i.e. the time between two 180° pulses in the Carr-Purcell-Meiboom-Gill (CPMG) pulse sequence we used in all our experiments. As at 25 °C (the temperature chosen for samples characterization) D = 2.5 × 10^{-9} m^2/s and, according to the information coming from the LF-NMR supplier (Bruker), we have $\Delta G < 10^{-2}$ T/m, it turns out that $1/T_{2D}$ is about 0.003% of $1/T_{2,H2O}$, i.e., it is negligible.

According to Brownstein and Tarr (1979), who dealt with spherical or cylindrical pores, and Chui et al. (1995), who extended the Brownstein and Tarr (1979) approach to fibrous systems such as gels (they defined the concept of "fiber cell", a cylindrical water volume surrounding each polymeric fiber), in Eq. (B.6) only the first addendum matters when fast diffusion conditions are attained. Fast diffusion occurs when water self-diffusion coefficient (D) is high, i.e. when the rate of diffusion (D) is high in comparison to the rate of magnetization loss $\mathscr{M}R$ at solid surface (pore wall or polymeric fiber surface. R represents pore radius or fiber cell radius). Indeed, in this situation there will be a rapid exchange between water molecules near the solid surface (pore wall or polymeric fiber surface), the so-called bound water, and the bulk or free water, i.e. water molecules far from the solid surface. Thus, when $\mathscr{M}R/D \ll 1$ (the typical situation met in hydrogels (Chui et al., 1995)), water relaxation inside the fiber cell is mono exponential and only one relaxation time is needed to describe $M_{xy}(t)$ decay. As in real hydrogels there will surely exist fiber cells characterized by different S/V ratios, the value of $(1/T_2)_m$ will be the averaged value competing to all the different kinds of fiber cells (each one characterized by only one spin-spin relaxation time). The implementation of the Chui model by Scherer (Scherer, 1994) allowed to consider a more realistic arrangement of the three-dimensional fibrous network of hydrogels. Indeed, he considered cubical, tetrahedral or octahedral arrangements. The simplification of this approach (Abrami et al., 2018), finally allowed to provide a simple, although powerful, expression of the S/V in term as function of the (cubical) mesh size (ε) and the polymer volume fraction in the gel (see Eq. (6)).

Appendix C. Supplementary data

The following is the supplementary data related to this article. The Eq. (12) parameters are presented. Hydrogels samples and experimental values of shear modulus G, their crosslink density ρ_x values and average relaxation time T_{2m} are shown. Parity plots for different hydrogel systems (comparison of experimental and calculated crosslink density of hydrogel samples) are illustrated. The spectrum of relaxation times distribution are demonstrated. Supplementary data to this article can be found online at doi:https://doi.org/10.1016/j.carbpol.2021.118895.

References

Abrami, M., D'Agostino, I., Milcovich, G., Fiorentino, S., Farra, R., Asaro, F., Lapasin, R., Grassi, G., & Grassi, M. (2014). Physical characterization of alginate–Pluronic F127 gel for endoluminal NABDs delivery. *Soft Matter, 10*, 729–737. https://doi.org/10.1039/c3sm51873f

Abrami, M., Chiarappa, G., Farra, R., Grassi, G., Marizza, P., & Grassi, M. (2018). Use of low-field NMR for the characterization of gels and biological tissues. *ADMET and DMPK, 6*(1), 34. https://doi.org/10.5599/admet.6.1.430

Abrami, M., Siviello, C., Grassi, G., Larobina, D., Grassi, M., & M.. (2019). Investigation on the thermal gelation of Chitosan/β-glycerophosphate solutions. *Carbohydrate Polymers, 214*, 110–116. https://doi.org/10.1016/j.carbpol.2019.03.015

Afghah, F., Altunbek, M., Dikyol, C., & Koc, B. (2020). Preparation and characterization of nanoclay-hydrogel composite support-bath for bioprinting of complex structures. *Scientific Reports, 10*(1), 1–13. https://doi.org/10.1038/s41598-020-61606-x

Ahmed, E. M. (2015). Hydrogel: Preparation, characterization, and applications: A review. *Journal of Advanced Research, 6*(2), 105–121. https://doi.org/10.1016/j.jare.2013.07.006. Elsevier B.V.

Amsden, B. (1998). Solute diffusion within hydrogels. *Mechanisms and Models Macromolecules, 31*, 8382–8395. https://doi.org/10.1021/ma980765f

Andrade Batista, R., Perez Espitia, P. J., De Souza, J., Quintans, S., Machado Freitas, M., Cerqueira, M.Â., Teixeira, J. A., & Cardoso, J. C. (2018). Hydrogel as an alternative structure for food packaging systems. *Carbohydrate Polymers, 205*, 106–116. https://doi.org/10.1016/j.carbpol.2018.10.006

Brownstein, K. R., & Tarr, C. E. (1979). Importance of classical diffusion in NMR studies of water in biological cells. *Physical Review A, 19*, 2446–2453. PhysRevA.19.2446.

Bruck, S. D. (1961). Extension of the flory-rehner theory of swelling to an anisotropic polymer system. *Journal of Research of the National Bureau of Standards Section A: Physics and Chemistry, 65A*(6), 485. https://doi.org/10.6028/jres.065a.051

Carr, D. A., & Peppas, N. A. (2009). Molecular structure of physiologically-responsive hydrogels controls diffusive behavior. *Macromolecular Bioscience, 9*(5), 497–505. https://doi.org/10.1002/mabi.200800235

Chen, G., Tang, W., Wang, X., Zhao, X., Chen, C., & Zhu, Z. (2019). Applications of hydrogels with special physical properties in biomedicine. *Polymers, 11*(9). https://doi.org/10.3390/polym11091420

Chui, M. M., Phillips, R. J., & McCarthy, M. J. (1995). Measurement of the porous microstructure of hydrogels by nuclear magnetic resonance. *Journal of Colloid and Interface Science, 174*, 336–344. https://doi.org/10.1006/jcis.1995.1399

Coates, G. R., Xiao, L. L., & Prammer, M. G. (1999). *NMR logging principles and application*. Houston: Halliburton Energy Services Publication.

Coviello, T., Palleschi, A., Grassi, M., Matricardi, P., Bocchinfuso, G., & Alhaique, F. (2005). Scleroglucan: A versatile polysaccharide for modified drug delivery. *Molecules, 10*(1), 6–33. https://doi.org/10.3390/10010006

Coviello, T., Matricardi, P., Alhaique, F., Farra, R., Tesei, G., Fiorentino, S., Asaro, F., Milcovich, G., & Grassi, M. (2013). Guar gum/borax hydrogel: Rheological, low field NMR and release characterizations. *Express Polymer Letters, 7*(9), 733–746. https://doi.org/10.3144/expresspolymlett.2013.71

Curvello, R., & Garnier, G. (2020). Cationic cross-linked nanocellulose-based matrices for the growth and recovery of intestinal organoids. *Biomacromolecules, 22*(2), 701–709. https://doi.org/10.1021/acs.biomac.0c01510

Das, D., & Pal, S. (2015). Modified biopolymer-dextrin based crosslinked hydrogels: Application in controlled drug delivery. *RSC Advances, 5*(32), 25014–25050. https://doi.org/10.1039/c4ra16103c

Descallar, F. B. A., & Shingo Matsukawa, S. (2020). Change of network structure in agarose gels by aging during storage studied by NMR and electrophoresis. *Carbohydrate Polymers, 245*, Article 116497. https://doi.org/10.1016/j.carbpol.2020.116497

Drageta, K. I., GåserØd, O., Aunea, I., Andersen, P. O., Storbakken, B., Stokke, B. T., & SmidsrØd, O. (2001). Effects of molecular weight and elastic segment flexibility on syneresis in Ca-alginate gels. *Food Hydrocolloids, 15*(4–6), 485–490. https://doi.org/10.1016/S0268-005X(01)00046-7

Drury, J. L., & Mooney, D. J. (2003). Hydrogels for tissue engineering: Scaffold design variables and applications. *Biomaterials, 24*(24), 4337–4351. https://doi.org/10.1016/S0142-9612(03)00340-5

Fanesi, G., Abrami, M., Zecchin, F., Giassi, I., Ferro, E. D., Boisen, A., Grassi, G., Bertoncin, P., Grassi, M., & Marizza, P. (2018). Combined used of rheology and LF-NMR for the characterization of PVP-alginates gels containing liposomes. *Pharmaceutical Research, 35*(9). https://doi.org/10.1007/s11095-018-2427-0, 171/1-171/11.

French, A. D. (2017). Glucose, not cellobiose, is the repeating unit of cellulose and why that is important. *Cellulose, 24*(11), 4605–4609. https://doi.org/10.1007/S10570-017-1450-3

Goy, C. B., Chaile, R. E., & Madrid, R. E. (2019). Microfluidics and hydrogel: A powerful combination. *Reactive and Functional Polymers, 145*, Article 104314. https://doi.org/10.1016/j.reactfunctpolym.2019.104314

Hecht, H., & Srebnik, S. (2016). Structural characterization of sodium alginate and calcium alginate. *Biomacromolecules, 17*(6), 2160–2167. https://doi.org/10.1021/acs.biomac.6b00378

Ho, T. T. T., Zimmermann, T., Hauert, R., & Caseri, W. (2011). Preparation and characterization of cationic nanofibrillated cellulose from etherification and high-shear disintegration processes. *Cellulose, 18*(6), 1391–1406. https://doi.org/10.1007/s10570-011-9591-2

Hoare, T. R., & Kohane, D. S. (2008). Hydrogels in drug delivery: Progress and challenges. *Polymer, 49*(8), 1993–2007. https://doi.org/10.1016/j.polymer.2008.01.027. Elsevier BV.

Homayouni, A., Ehsani, M. R., Azizi, A., Saeid Yarmand, M., & Razavi, S. H. (2007). Effect of lecithin and calcium chloride solution on the microencapsulation process yield of calcium alginate beads (English) *Iranian Polymer Journal, 16*(9) http://journal.ippi.ac.ir.

Isogai, A., Saito, T., & Fukuzumi, H. (2011). *3*(1), 71–85. https://doi.org/10.1039/c0nr00583e

Jaeger, F., Shchegolikhina, A., Van Asc, H., & Schaumann, G. E. (2010). Proton NMR relaxometry as a useful tool to evaluate swelling processes in peat soils. *Open Magnetic Resonance Journal, 3*, 27–45. https://doi.org/10.2174/1874769801003010027

Kirchhof, S., Abrami, M., Messmann, V., Hammer, N., Goepferich, A. M., Grassi, M., & Brandl, F. P. (2015). Diels-Alder hydrogels for controlled antibody release: Correlation between mesh size and release rate. *Molecular Pharmaceutics, 12*(9), 3358–3368. https://doi.org/10.1021/acs.molpharmaceut.5b00375

Klemm, D., Kramer, F., Moritz, S., Lindström, T., Ankerfors, M., Gray, D., & Dorris, A. (2011). Nanocelluloses: A new family of nature-based materials. *Angewandte Chemie, International Edition, 50*(24), 5438–5466. https://doi.org/10.1002/anie.201001273

Kopač, T., Ručigaj, A., & Krajnc, M. (2020). The mutual effect of the crosslinker and biopolymer concentration on the desired hydrogel properties. *International Journal of Biological Macromolecules, 159*, 557–569. https://doi.org/10.1016/j.ijbiomac.2020.05.088

Kopač, T., Krajnc, M., & Ručigaj, A. (2021). A mathematical model for pH-responsive ionically crosslinked TEMPO nanocellulose hydrogel design in drug delivery systems. *International Journal of Biological Macromolecules, 168*, 695–707. https://doi.org/10.1016/j.ijbiomac.2020.11.126

Lapasin, R., Abrami, M., Grassi, M., & Šebenik, U. (2017). Rheology of laponite-scleroglucan hydrogels. *Carbohydrate Polymers, 168*, 290–300. https://doi.org/10.1016/j.carbpol.2017.03.068

Li, X., Li, Y., Chen, C., Zhao, D., Wang, X., Zhao, L., Shi, H., Ma, G., & Su, Z. (2015). Pore size analysis from low field NMR spin–spin relaxation measurements of porous microspheres. *Journal of Porous Materials, 22*, 11–20. https://doi.org/10.1007/s10934-014-9864-x

Li, Y., Li, X., Chen, C., Zhao, D., Sub, Z., Mab, G., & Yu, R. (2016). A rapid, non-invasive and non-destructive method for studyingswelling behavior and microstructure variations of hydrogels. *Carbohydrate Polymers, 151*, 1251–1260. https://doi.org/10.1016/j.carbpol.2016.06.054

Liang, L., Bhagia, S., Li, M., Huang, C., & Ragauskas, A. J. (2020). Cross-linked nanocellulosic materials and their applications. *ChemSusChem, 13*(1), 78–87. https://doi.org/10.1002/cssc.201901676

Liang, Y., Xue, J., Du, B., & Nie, J. (2019). Ultrastiff, tough, and healable ionic-hydrogen bond cross-linked hydrogels and their uses as building blocks to construct complex hydrogel structures. *ACS Applied Materials and Interfaces, 11*(5), 5441–5454. https://doi.org/10.1021/acsami.8b20520

Lin, N., & Dufresne, A. (2014). Nanocellulose in biomedicine: Current status and future prospect. *European Polymer Journal, 59*, 302–325. https://doi.org/10.1016/j.eurpolymj.2014.07.025

Lin, N., Bruzzese, C., & Dufresne, A. (2012). TEMPO-oxidized nanocellulose participating as crosslinking aid for alginate-based sponges. *ACS Applied Materials and Interfaces, 4*(9), 4948–4959. https://doi.org/10.1021/am301325r

Lundahl, M. J., Berta, M., Ago, M., Stading, M., & Rojas, O. J. (2018). Shear and extensional rheology of aqueous suspensions of cellulose nanofibrils for biopolymer-assisted filament spinning. *European Polymer Journal, 109*, 367–378. https://doi.org/10.1016/j.eurpolymj.2018.10.006

Maestri, C. A., Abrami, M., Hazan, S., Chistè, E., Golan, Y., Rohrer, J., Bernkop-Schnürch, A., Grassi, M., Scarpa, M., & Bettotti, P. (2017). Role of sonication pre-treatment and cation valence in the sol-gel transition of nano-cellulose suspensions. *Scientific Reports, 7*(1), 1–10. https://doi.org/10.1038/s41598-017-11649-4

Mahinroosta, M., Jomeh Farsangi, Z., Allahverdi, A., & Shakoori, Z. (2018). Hydrogels as intelligent materials: A brief review of synthesis, properties and applications. *Materials Today Chemistry, 8*, 42–55. https://doi.org/10.1016/j.mtchem.2018.02.004

Manga, R. D., & Jha, P. K. (2017). Mathematical models for controlled drug release through pH-responsive polymeric hydrogels. *Journal of Pharmaceutical Sciences, 106*(2), 629–638. https://doi.org/10.1016/j.xphs.2016.10.019

Marizza, P., Abrami, M., Keller, S. S., Posocco, P., Laurini, E., Goswami, K., Skov, A. L., Boisen, A., Larobina, D., Grassi, G., & Grassi, M. (2016). Synthesis and characterization of UV photocrosslinkable hydrogels with poly(N-vinyl-2-pyrrolidone): Determination of the network mesh size distribution. *International Journal of Polymeric Materials and Polymeric Biomaterials, 65*, 516–525. https://doi.org/10.1080/00914037.2015.1129964

Mehandzhiyski, A. Y., Riccardi, E., Van Erp, T. S., Koch, H., Åstrand, P. O., Trinh, T. T., & Grimes, B. A. (2015). Density functional theory study on the interactions of metal ions with long chain deprotonated carboxylic acids. *Journal of Physical Chemistry A, 119*(40), 10195–10203. https://doi.org/10.1021/acs.jpca.5b04136

Meiboom, S., & Gill, D. (1958). Modified spin-echo method for measuring nuclear relaxation times. *The Review of Scientific Instruments, 29*, 688–691. https://doi.org/10.1063/1.1716296

Nazmabadi, M., Shirdast, A., Sharif, A., & Aalaie, J. (2020). Aqueous/brine solutions viscosity and surface properties of hydrophobically modified scleroglucans: Role of grafted chain length. *Carbohydrate Polymers, 229*, Article 115519. https://doi.org/10.1016/j.carbpol.2019.115519

Paolicelli, P., Varani, G., Pacelli, S., Ogliani, E., Nardoni, M., Petralito, S., Adrover, A., & Casadei, M. A. (2017). Design and characterization of a biocompatible physical hydrogel based on scleroglucan for topical drug delivery. *Carbohydrate Polymers, 174*, 960–969. https://doi.org/10.1016/j.carbpol.2017.07.008

Park, K., Dawson, J. I., Oreffo, R. O. C., Kim, Y. H., & Hong, J. (2020). Nanoclay-polyamine composite hydrogel for topical delivery of nitric oxide gas via innate gelation characteristics of laponite. *Biomacromolecules, 21*(6), 2096–2103. https://doi.org/10.1021/acs.biomac.0c00086

Patiño-Masó, J., Serra-Parareda, F., Tarrés, Q., Mutjé, P., Espinach, F. X., & Delgado-Aguilar, M. (2019). TEMPO-oxidized cellulose nanofibers: A potential bio-based superabsorbent for diaper production. *Nanomaterials, 9*(9). https://doi.org/10.3390/nano9091271

Peppas, N. A., Bures, P., Leobandung, W., & Ichikawa, H. (2000). Hydrogels in pharmaceutical formulations. *European Journal of Pharmaceutics and Biopharmaceutics, 50*(1), 27–46. https://doi.org/10.1016/S0939-6411(00)00090-4

Rosiak, J. M., & Yoshii, F. (1999). Hydrogels and their medical applications. *Nuclear Instruments and Methods in Physics Research, Section B: Beam Interactions with Materials and Atoms, 151*(1–4), 56–64. https://doi.org/10.1016/S0168-583X(99)00118-4

Ruzicka, B., & Zaccarelli, E. (2011). A fresh look at the laponite phase diagram. *Soft Matter, 7*(4), 1268–1286. https://doi.org/10.1039/c0sm00590h

Saalwachter, K. (2003). Detection of heterogeneities in dry and swollen polymer networks by proton low-field NMR spectroscopy. *JACS, 125*, 14684–14685. https://doi.org/10.1021/ja038278p

Saalwachter, K. (2007). Proton multiple-quantum NMR for the study of chain dynamics and structural constraints in polymeric soft materials. *Progress in NMR Spectroscopy, 51*, 1–35. https://doi.org/10.1016/j.pnmrs.2007.01.001

Saalwachter, K., Chasse, W., & Sommer, J. U. (2013). Structure and swelling of polymer networks: Insights from NMR. *Soft Matter, 29*, 6587–6593. https://doi.org/10.1039/c3sm50194a

Scherer, G. W. (1994). Hydraulic radius and mesh size of gels. *Journal of Sol-Gel Science and Technology, 1*, 285–291. https://doi.org/10.1007/BF0048617

Šebenik, U., Krajnc, M., Alič, B., & Lapasin, R. (2019). Ageing of aqueous TEMPO-oxidized nanofibrillated cellulose dispersions: A rheological study. *Cellulose, 26*(2), 917–931. https://doi.org/10.1007/s10570-018-2128-1

Šebenik, U., Lapasin, R., & Krajnc, M. (2020). Rheology of aqueous dispersions of laponite and TEMPO-oxidized nanofibrillated cellulose. *Carbohydrate Polymers, 240*, Article 116330. https://doi.org/10.1016/j.carbpol.2020.116330

Sheu, S. Y., Yang, D. Y., Selzle, H. L., & Schlag, E. W. (2003). Energetics of hydrogen bonds in peptides. *Proceedings of the National Academy of Sciences of the United States of America, 100*(22), 12683–12687. https://doi.org/10.1073/pnas.2133366100

Valentın, J. L., Lopez, D., Hernandez, R., Mijangos, C., & Saalwachter, K. (2009). Structure of Poly(vinyl alcohol) cryo-hydrogels as studied by proton low-field NMR spectroscopy. *Macromolecules, 42*, 263–272. https://doi.org/10.1021/ma802172g

Wang, K. L., Burban, J. H., & Cussler, E. L. (1993). Hydrogels as separation agents. *Advances in Polymer Science, 110*, 66–79. https://doi.org/10.1007/bfb0021129

Way, A. E., Hsu, L., Shanmuganathan, K., Weder, C., & Rowan, S. J. (2012). pH-responsive cellulose nanocrystal gels and nanocomposites. *ACS Macro Letters, 1*(8), 1001–1006. https://doi.org/10.1021/mz3003006

Wisniewska, M. A., Seland, J. G., & Wang, W. (2018). Determining the scaling of gel mesh size with changing crosslinker concentration using dynamic swelling, rheometry, and PGSE NMR spectroscopy. *Journal of Applied Polymer Science, 46695*, 1–10. https://doi.org/10.1002/APP.46695

Xu, H., Liu, Y., Xie, Y., Zhu, E., Shi, Z., Yang, Q., & Xiong, C. (2019). Doubly cross-linked nanocellulose hydrogels with excellent mechanical properties. *Cellulose, 26*(16), 8645–8654. https://doi.org/10.1007/s10570-019-02689-2

Zinge, C., & Kandasubramanian, B. (2020). Nanocellulose based biodegradable polymers. *European Polymer Journal, 133*, Article 109758. https://doi.org/10.1016/j.eurpolymj.2020.109758